

SOL-844 *Sup Design*
Bragg

FWDC-9-41-341106

CONCEPTUAL DESIGN OF A HEAT PIPE SOLAR RECEIVER GAS
TURBINE PLANT

Final Report

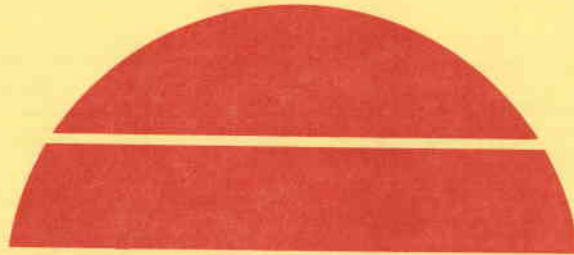
By
Giovanni Carli

8450 FILE COPY

September 15, 1978

Work Performed Under Contract No. EY-76-C-02-2839

Foster Wheeler Development Corporation
Livingston, New Jersey



U.S. Department of Energy

Cat No: 22.0105



Solar Energy

9

DISCLAIMER

"This book was prepared as an account of work sponsored by an agency of the United States Government. Neither the United States Government nor any agency thereof, nor any of their employees, makes any warranty, express or implied, or assumes any legal liability or responsibility for the accuracy, completeness, or usefulness of any information, apparatus, product, or process disclosed, or represents that its use would not infringe privately owned rights. Reference herein to any specific commercial product, process, or service by trade name, trademark, manufacturer, or otherwise, does not necessarily constitute or imply its endorsement, recommendation, or favoring by the United States Government or any agency thereof. The views and opinions of authors expressed herein do not necessarily state or reflect those of the United States Government or any agency thereof."

This report has been reproduced directly from the best available copy.

Available from the National Technical Information Service, U. S. Department of Commerce, Springfield, Virginia 22161.

Price: Paper Copy \$9.00
Microfiche \$3.50

FINAL REPORT

CONCEPTUAL DESIGN OF A
HEAT PIPE SOLAR RECEIVER
GAS TURBINE PLANT

Prepared for

Dynatherm Corporation
Cockeysville, Maryland 21030

By

Giovanni Carli
Project Manager

September 15, 1978

FWDC No. 9-41-341106



FOSTER WHEELER DEVELOPMENT CORPORATION

12 Peach Tree Hill Road, Livingston, New Jersey 07039

FOSTER WHEELER DEVELOPMENT CORPORATION

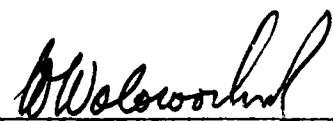
REF.: 9-41-341106

DATE: September 15, 1978

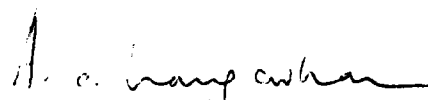
The contents of this report have been reviewed and approved by:



R. J. Zoschak
Technical Director, Applied
Thermodynamics Research



W. Wolowodiuk
Manager, Applied Thermodynamics
and Process Department



A. C. Gangadharan
Manager, Engineering Science
and Technology Department

TABLE OF CONTENTS

<u>Section</u>		<u>Page</u>
	ABSTRACT	vii
1	INTRODUCTION	1-1
2	CYCLE SELECTION	2-1
3	SELECTION OF OPERATING CONDITIONS	3-1
	3.1 Turbine-Inlet Temperature	3-1
	3.2 Plant Size	3-1
	3.3 Description of the Selected Cycle	3-2
4	DESCRIPTION OF THE PLANT	4-1
	4.1 Collector Subsystem	4-1
	4.2 Receiver Subsystem	4-3
	4.3 Interconnecting Piping	4-11
	4.4 Electric Power Generation Subsystem	4-12
	4.5 Tower Subsystem	4-15
5	PERFORMANCE ANALYSIS	5-1
	5.1 Plant Energy Chain	5-1
	5.2 Heat-Flux Profiles	5-2
	5.3 Thermal/Hydraulic Analysis	5-4
6	STRUCTURAL ANALYSES	6-1
	6.1 Loading Conditions	6-1
	6.2 Receiver Shell	6-2
	6.2.1 Front, Side, and Rear Walls	6-2
	6.2.2 Inlet and Outlet Heads	6-5
	6.3 Heat Pipes	6-6
	6.3.1 Stress Analysis	6-6
	6.3.2 Evaluation of Dynatherm Heat Pipe Test	6-7
	6.4 Inlet and Outlet Pipes	6-9
	6.5 Support Platform	6-10

TABLE OF CONTENTS (Cont)

<u>Section</u>		<u>Page</u>
7	HYBRID OPERATION CONSIDERATIONS	7-1
8	PLANT CAPITAL COST	8-1
9	CONCLUSIONS	9-1
10	REFERENCES	10-1

LIST OF ILLUSTRATIONS

<u>Figure</u>		<u>Page</u>
2.1	Open-Cycle Gas Turbine--Simple Cycle	2-2
2.2	Open-Cycle Gas Turbine--Regenerative Cycle	2-3
2.3	Closed-Cycle Gas Turbine	2-3
2.4	Gas Cycle Efficiency	2-5
2.5	Receiver Heat Losses	2-6
2.6	Overall System Efficiency	2-7
3.1	Regenerative Open Air Cycle Flow Diagram	3-4
4.1	Plot Plan of Collector Field	4-2
4.2	Cavity Receiver Configuration	4-5
4.3	Panel Configuration	4-7
4.4	Schematic of Heat Pipe	4-8
4.5	Typical Heat Pipe Layout	4-9
4.6	Schematic of Heat Pipe Installation	4-10
4.7	Gas Turbine Cross-Section	4-14
4.8	Plan View of Platform Showing Components Location	4-17
5.1	Plant Energy Flow Diagram	5-2
5.2	Plant Energy Chain	5-3
5.3	Incident Heat Flux to Panels	5-6
5.4	Airflow Distribution to Panels	5-8
7.1	Hybrid, Open Brayton Cycle Central Receiver System	7-2

LIST OF TABLES

<u>Table</u>		<u>Page</u>
3.1	Operating and Design Requirements for 10-MWe Plant	3-3
4.1	Heliostat Field Data	4-3
4.2	Estimated Component Weight	4-16
5.1	Incident Heat-Flux Density to Panel Zones	5-5
5.2	Incident Average Energy to Panel Zones	5-7
5.3	Average Energy Transport Requirements	5-9
5.4	Temperature of Air in the Panel	5-10
5.5	Average Condensing Section Heat Pipe Mean-Wall Temperature	5-11
6.1	Stresses in Front Plate	6-3
6.2	Stresses in Rear Plate	6-4
6.3	Stresses in Side Panels	6-4
6.4	Stresses in the Inlet Head	6-5
6.5	Stresses in the Outlet Head	6-6
6.6	Allowable Heat Fluxes for an Axisymmetrically Heated Inconel 601 Tube vs. Inner Fluid Temperature	6-7
6.7	Test Specimen and Loading Parameters	6-8
6.8	Thermal Stresses in Heat Pipe Test Conducted at Dynatherm	6-9
6.9	Stresses in Inlet and Outlet Pipes	6-10
8.1	Capital Cost Expenditures	8-3

ABSTRACT

A conceptual design for a 10-MWe Heat Pipe Central Receiver Gas-Turbine Power Plant has been developed. The heat pipe central solar receiver uses heat pipes to transform the concentrated high solar heat flux at the receiver into a lower heat flux compatible with gas heat-transfer systems. Several Brayton cycles were studied to determine which cycles and operating conditions are technically and economically most viable for a central receiver power plant. A regenerative open-gas cycle with an inlet turbine temperature of 816°C (1500°F) was selected.

The turbine-generator and receiver are located at the top of a steel tower, with a north field of 2-axis tracking heliostats. The system can be adapted for operation as a hybrid plant, providing a higher level of availability and a dependable generating capacity--important considerations from the utility point of view.

The predicted cycle efficiency is 33 to 38 percent, and the overall solar-to-electric efficiency is 19.1 to 22.3 percent. Capital cost of the plant is estimated to be in the \$1,947 to \$2,002/kW range, depending on the assumed cost for the collector system. Compared with a water/steam solar system, estimated costs in mid-1978 dollars are lower and plant efficiency is superior.

Section 1

INTRODUCTION

This final report presents the work performed by Foster Wheeler Development Corporation (FWDC) during the period of March 1976 to August 1978 under a subcontract to Dynatherm Corporation (Subcontract No. D-1966). The work was sponsored by the Department of Energy (Contract No. EY-76-C-02-2839).

The primary objectives of this project were to develop the conceptual design of a high-temperature, gas-cooled heat pipe central receiver power plant that has a utility-type gas turbine as the prime mover, to determine the technical and economic feasibility of such a plant, and to obtain preliminary overall cost estimates of the plant.

The main advantages of a gas solar plant over the more conventional water/steam solar plant are the improved turbine-cycle and receiver efficiencies, which minimize the collector field area required for a given electrical output. Higher cycle efficiency results from the high receiver-outlet air temperature; increased receiver efficiency results from the excellent heat-transfer capabilities of the heat pipes, which allow a higher heat flux on the receiver absorbing surfaces. This higher heat flux reduces receiver heating surface, thereby reducing receiver heat losses. Furthermore, the gas solar system can be easily developed for hybrid operation, thus increasing system availability and dependability and avoiding the need to develop costly and untried thermal storage systems.

The initial phase of the program concentrated on the conceptual design of the receiver to establish the performance requirements for the heat pipes. The design goal was a conceptual design of a receiver with a 30-year lifetime.

Several receiver shapes were analyzed, and parametric data were developed to enable selection of a baseline receiver concept for more detailed analysis. A baseline design was selected by considering performance and cost. The design intentionally parallels the current design for a water/steam solar central receiver pilot plant to permit direct cost and performance comparisons between the two plants.

The limited funds available for this study restricted the number of trade-off studies conducted to select the optimum configuration of the plant. System data developed as part of the ongoing water/steam solar plant program were utilized as much as possible to maximize the use of these limited funds and to minimize duplication of efforts on systems common to these two types of plants.

Section 2
CYCLE SELECTION

During the early stages of this program a comparison of the trade-offs between performance and cost of several types of Brayton cycles was made to determine the most desirable cycles for a central solar receiver power plant. The primary objective of this preliminary evaluation was to investigate variations in cycle parameters and configurations. Factors considered were relative capital costs; energy-conversion efficiency; and complexity of design, operation, and control.

During this initial evaluation phase, no specific heat-flux profiles were provided. Consequently, reasonable values for peak and average heat fluxes were based on previous central receiver studies performed for the water/steam solar plants.

Bottoming cycles were eliminated as possible candidates because simplicity of design was considered important for a prototypical solar plant. Although combining a Brayton cycle with a bottoming cycle enhances efficiency, it was not considered here because of the increased complexity of the system. Bottoming also adversely affects construction time, amount of site labor, operation, and control. A final system design study would have to include a trade-off study of the increased system costs vs. the increase in efficiency.

Since the receiver design and development will be essentially unaffected by whether the system operates in a hybrid or stand-alone mode, the stand-alone

plant concept was selected instead of the hybrid concept in which the solar plant is coupled with a conventional fossil-fueled electric power plant.

After the preliminary evaluation, the three Brayton cycles remaining as potential candidates for the central solar receiver were:

- Simple open-cycle gas turbine
- Open-cycle gas turbine with regenerator
- Closed-cycle (helium) gas turbine.

The schematic diagrams of these three cycles are presented in Figures 2.1, 2.2, and 2.3 respectively. Trade-off studies were performed for the cycles, with consideration given to size, weight, cost, and performance of such cycle components as turbines, compressor, generators, and cooling towers. Since these components are commercially established in conventional power plants, the data were obtained on the basis of wide experience and, therefore, they are reasonably well-defined.

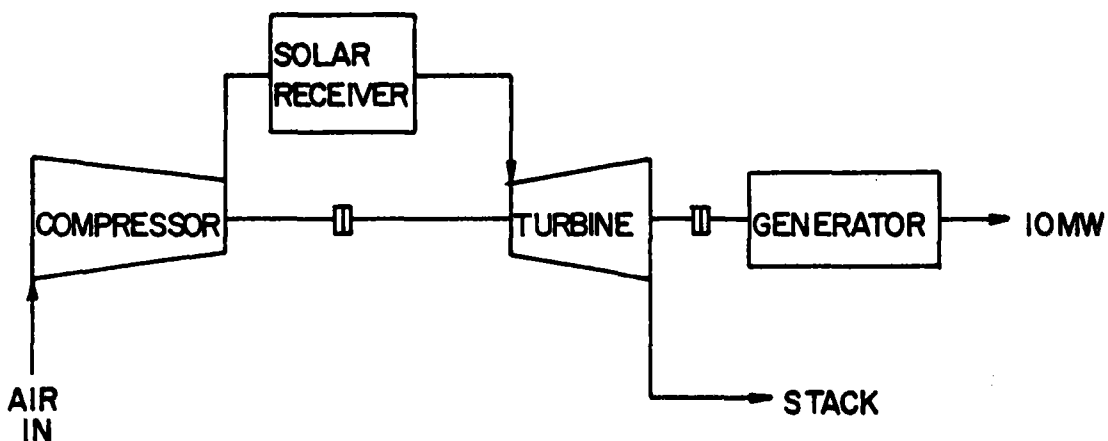


Figure 2.1 Open-Cycle Gas Turbine--Simple Cycle

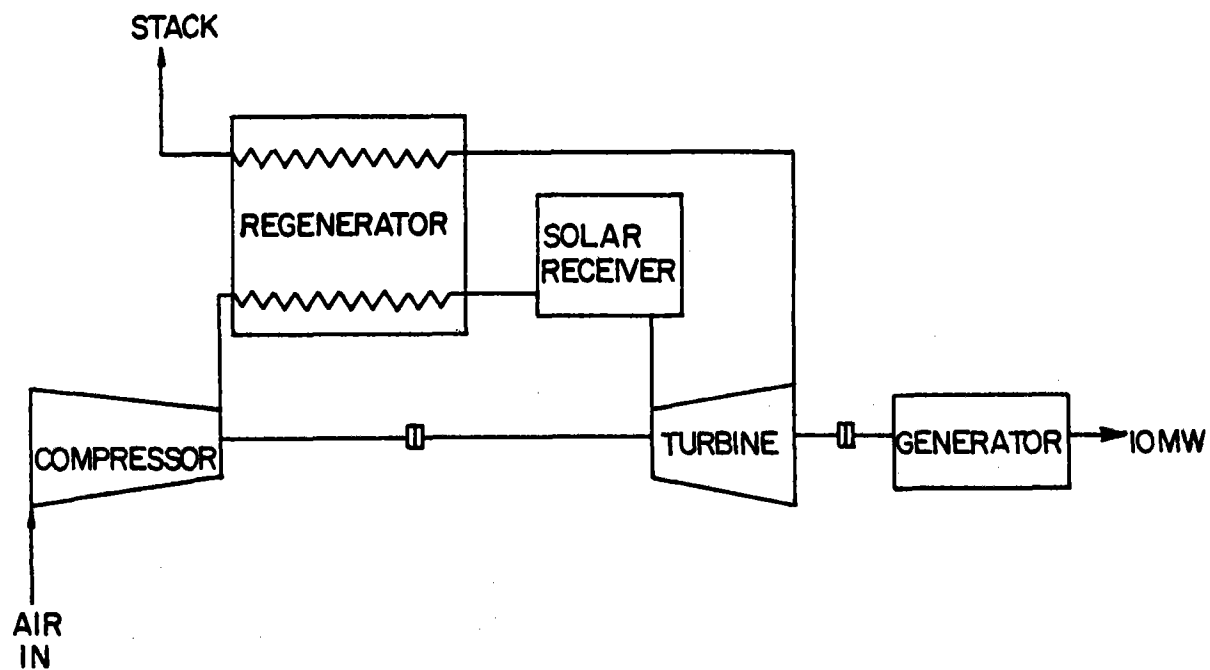


Figure 2.2 Open-Cycle Gas Turbine--Regenerative Cycle

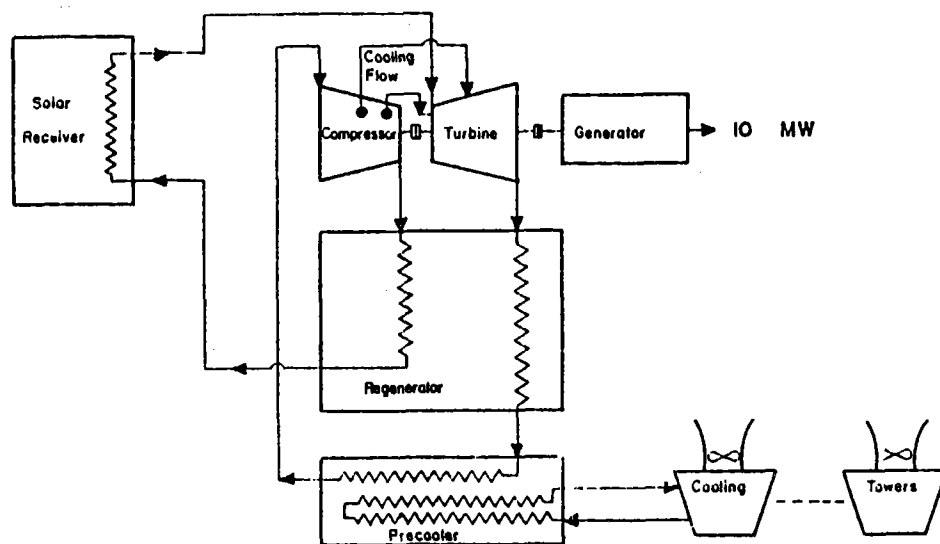


Figure 2.3 Closed-Cycle Gas Turbine

In a Brayton cycle, approximately two-thirds of the turbine output is used to drive the compressor. Thus the Brayton cycle is very sensitive to efficiency losses in the compressor as well as to pressure losses in the piping connecting the compressor to the receiver and the receiver to the turbine. As can be seen in Figure 2.4, in a Brayton cycle the efficiency increases with inlet turbine temperature,^{1*} and thus, the cycle efficiency is maximized by increasing the turbine-inlet gas temperature and by reducing the total pressure drop between the compressor outlet and the turbine inlet.

Normally, the turbine-inlet temperature and hence the cycle efficiency are determined by materials considerations. In a solar power plant, however, higher turbine inlet temperatures also mean increased heat losses from the receiver by reradiation and convection.

The heat losses for a cavity-type solar receiver were evaluated empirically. The analysis involved several simplifying assumptions:

- Reradiation losses were calculated assuming an emissivity of 1.
- Convection losses were calculated for a wind velocity of 24 km/h (15 mi/h).
- Conduction losses were assumed to be negligible, because they were held to a minimum with 0.3-m (12-in.)-thick insulation.

Results of the analysis are shown in Figure 2.5. The estimated values are consistent with published data. By combining Figures 2.4 and 2.5, an optimum turbine-inlet temperature can be obtained. Figure 2.6 shows that the

*Numbers designate references in Section 10.

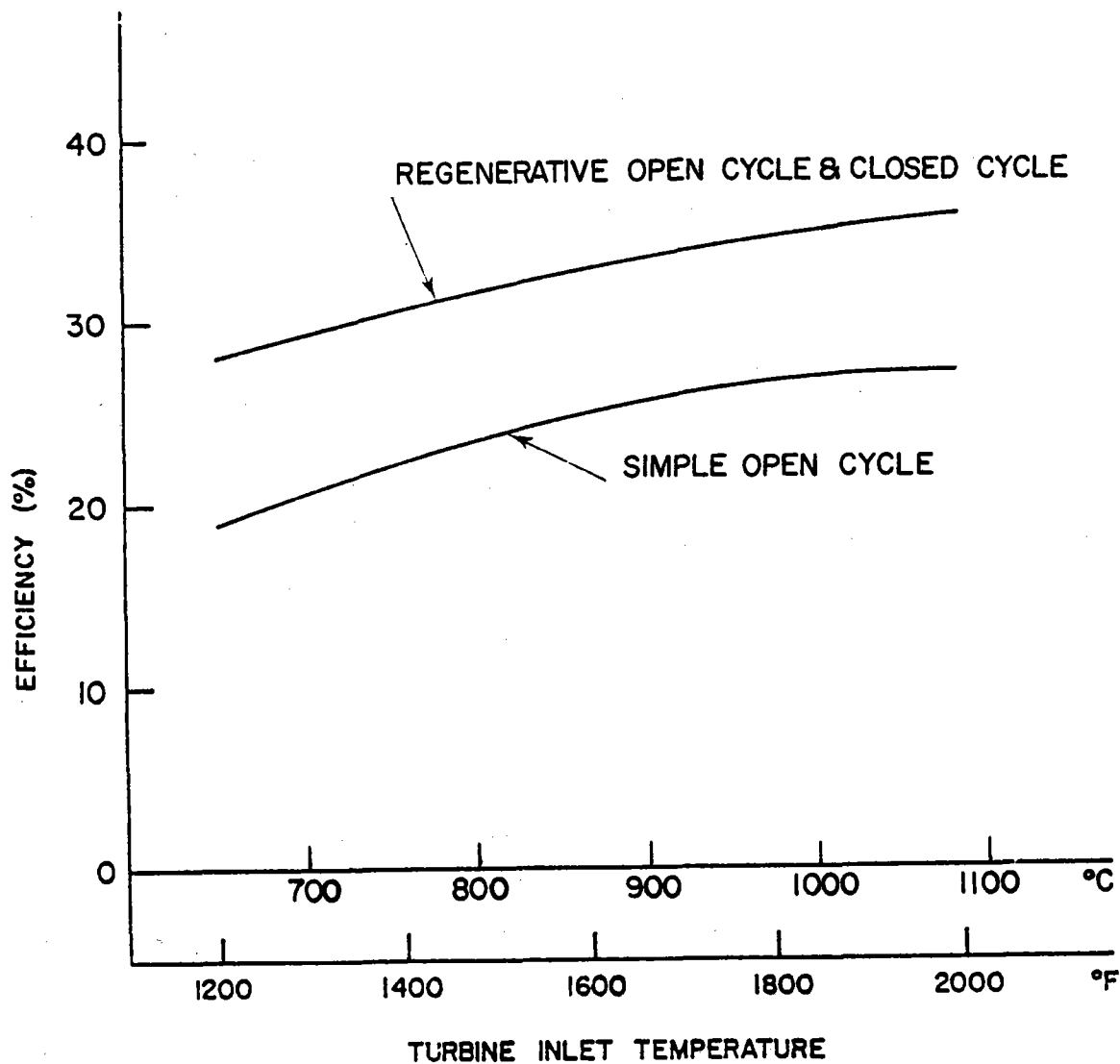


Figure 2.4 Gas Cycle Efficiency

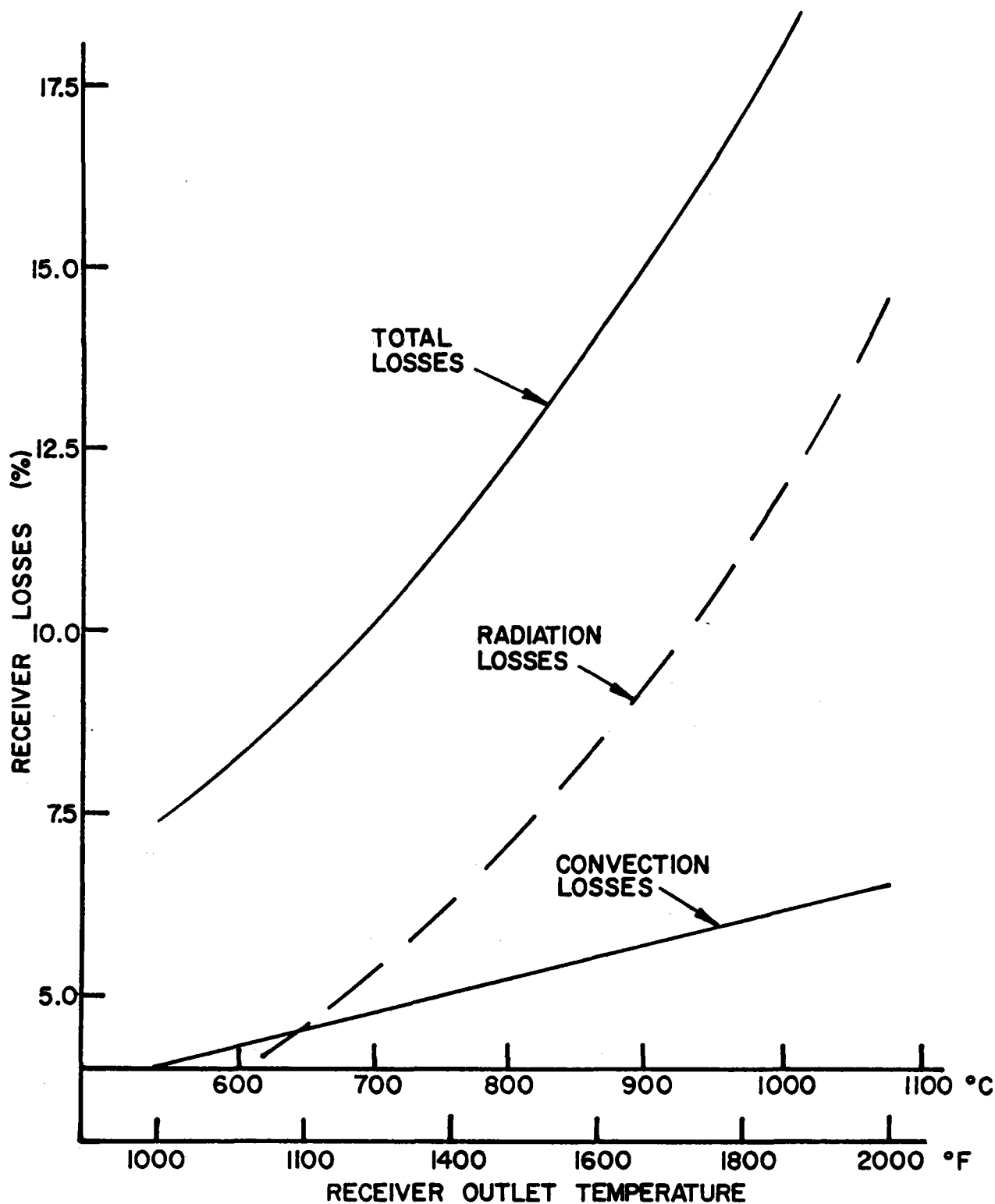


Figure 2.5 Receiver Heat Losses

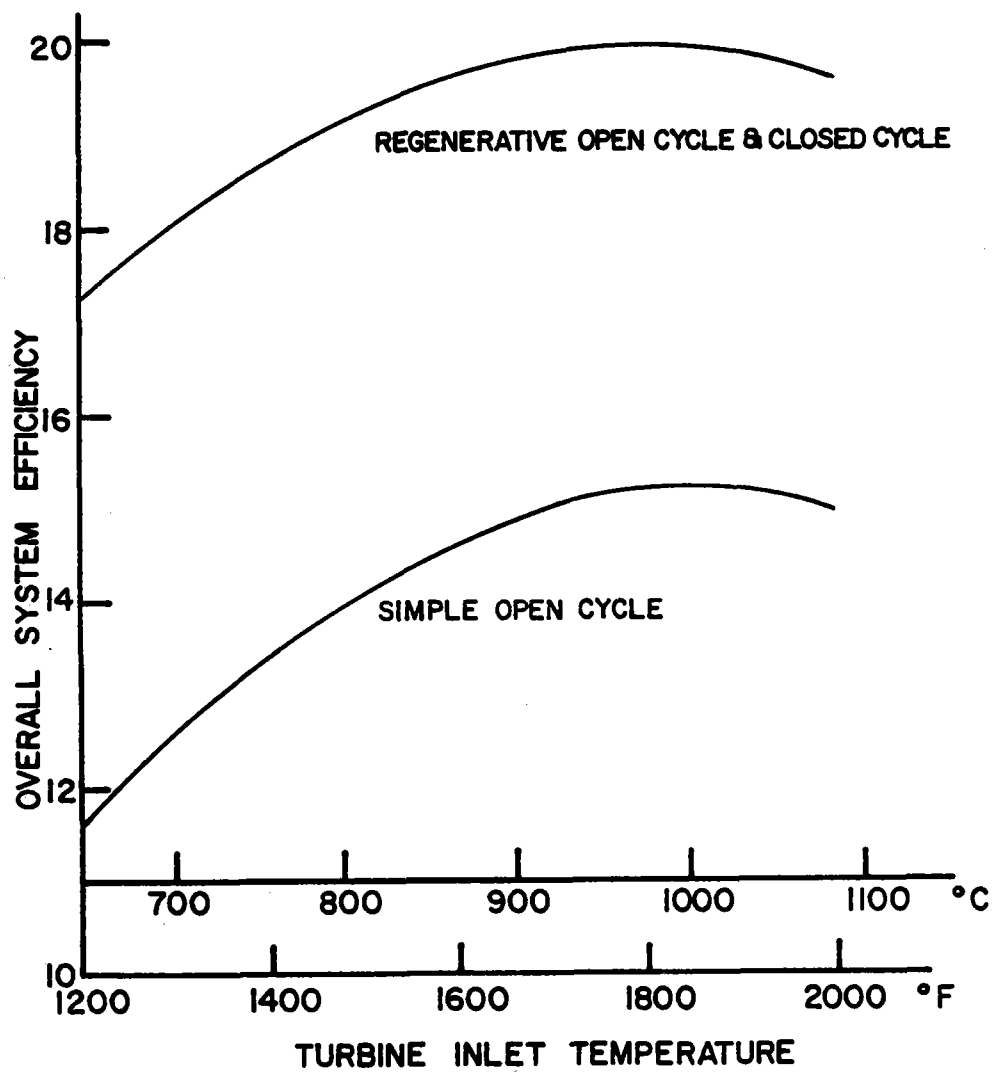


Figure 2.6 Overall System Efficiency

overall solar cycle efficiency (defined as the net electrical power generated divided by the solar energy to the mirrors) has an optimum value of approximately 20 percent for both the open-cycle gas turbine with regenerator and the closed-cycle (helium) gas turbine and a value of approximately 15 percent for the simple open-cycle gas turbine. Thus at optimum conditions the simple open cycle will require approximately 30 percent more heliostat field area than the other two cycles.

The design philosophy followed in the system selection was to emphasize thermal efficiency wherever possible in order to reduce collector system costs. The heliostat field constitutes the most expensive component in a solar plant; therefore, a reduction in the required heliostat field size will result in significant cost savings. Cost estimates show that the savings accrued by using an open-cycle gas turbine with a regenerator greatly exceed the additional cost of the regenerator.^{2,3} Thus the simple open-cycle gas turbine was eliminated as a potential candidate for the gas solar plant.

Systems trade-off analyses for the Energy Conversion Alternatives Study³ indicate that the cycle components (inlet and exhaust systems, compressor, turbine, generator, and regenerator) for a closed-cycle gas turbine weigh 10 times more than the components for an open-cycle gas turbine with regenerator. The cost comparison of the two cycles indicates that the closed cycle is again much more expensive than the open gas cycle, even when the less expensive water cooling towers are used in the closed cycle. Since availability of water is a severe constraint at most potential solar plant sites, the more expensive dry-cooling

towers will be required, making the closed cycle even less attractive. Furthermore, the closed cycle operates at high pressures, which combined with the high temperature of 815°C (1500°F) or more expected in the solar receiver, means serious design problems and a much heavier receiver and connecting ducts. Helium containment design problems are also a consideration in a closed cycle. Thus the closed cycle was eliminated from consideration for the gas solar plant.

Based on the above considerations, the open-cycle gas turbine with regenerator was selected as the cycle most technically and economically favorable for a central receiver solar Brayton cycle power plant.

Section 3

SELECTION OF OPERATING CONDITIONS

3.1 TURBINE-INLET TEMPERATURE

As seen in Figure 2.6, the overall plant efficiency (losses included) does not change significantly in the turbine-inlet temperature range of 816 to 980°C (1500 to 1800°F). For this reason and because conservative values are desirable in a prototypical plant, the 816°C (1500°F) turbine-inlet temperature was selected. From a materials standpoint, 816°C (1500°F) will be considered the upper limit. In this case higher temperatures, although resulting in a slightly higher efficiency, were considered undesirable when weighed against the resultant additional risks.

3.2 PLANT SIZE

A simple receiver module coupled with a 10-MWe turbine/generator has been selected as the conceptual size for this plant. The rationale for this selection is:

- The degree to which the plant will compare with other solar plants currently being designed was of prime concern. The current solar effort calls for the building and testing of a 10-MWe steam solar plant.⁴ By choosing a similar-sized gas solar plant, comparison and evaluation will be easier, and the same test facility can be used for both.
- Commercial components (turbine, compressor, generator, regenerator) with proven long-life reliability are available for 816°C (1500°F) inlet temperature in the 10-MWe size.
- The estimated weight for a 10-MWe plant (seismic considerations aside) allows all the components to be located with the receiver atop the tower, resulting in considerably lower piping cost and heat loss.

- The 10-MWe plant capacity selected is large enough for a valid demonstration of the system on a commercial scale, yet small enough to minimize capital risk.
- Establishing the turbine rated capacity permits the sizes of heliostat field, receiver, and tower to be determined.

Table 3.1 summarizes the full-load operating and design conditions that have been selected for this plant. The range of efficiencies shown represent the practical upper and lower limits. The selection of the optimum point within the range, which depends on the overall system costs, requires extensive trade-off cost analyses which were beyond the scope of this study.

The design requirements given in Table 3.1 are similar to those specified for the water/steam solar plants. A 30-year design life with 90-percent availability gives a total of approximately 13,000 start/stop cycles--10,000 daily starts with the remainder allocated to transients during the day.

3.3 DESCRIPTION OF THE SELECTED CYCLE

The schematic flow diagram for the selected cycle, an open air cycle with regenerator, is shown in Figure 3.1. As previously mentioned, this cycle was selected because of potentially higher cycle efficiency and reduced receiver weights and system costs.

Ambient air at 15.5°C (60°F) is delivered to a single-shaft, multistage, axial-flow compressor driven on a common shaft by the turbine. After being compressed by a factor of about 6 to 1, the air is directed to the regenerator, where it is further heated to about 443°C (829°F) by the turbine-exhaust gases. From this point, the air would normally enter a standard fossil-fuel combustor

Table 3.1 Operating and Design Requirements for 10-MWe Plant

Plant Performance:

Power to mirrors, MWt	45 - 51
Power to receiver, MWt	30 - 35
Radiation and convection losses, MWt	3 - 4
Power to air, MWt	27 - 31
Nominal net power output, MWe	10
Overall energy efficiency, %	19.2 - 22.3

Cycle Condition:

Compressor inlet temperature, °C (°F)	15.5 (60)
Turbine inlet temperature, °C (°F)	816 (1500)
Compressor inlet pressure, MPa (lb/in ² a)	0.1 (14.7)
Turbine inlet pressure, MPa (lb/in ² a)	0.57 (85)
Pressure ratio	6
Cycle efficiency range, %	33 - 38
Turbine efficiency, %	85 - 92
Compressor efficiency, %	80 - 88
Recuperator effectiveness, %	85 - 94
Flow, kg/s (lb/s)	67.3 (148) - 77.3 (170)

Design Requirements:

Plant cycles	13,000
Operational life, yr	30
Plant availability, %	90
Average wind velocity, km/h (mi/h)	24 (15)

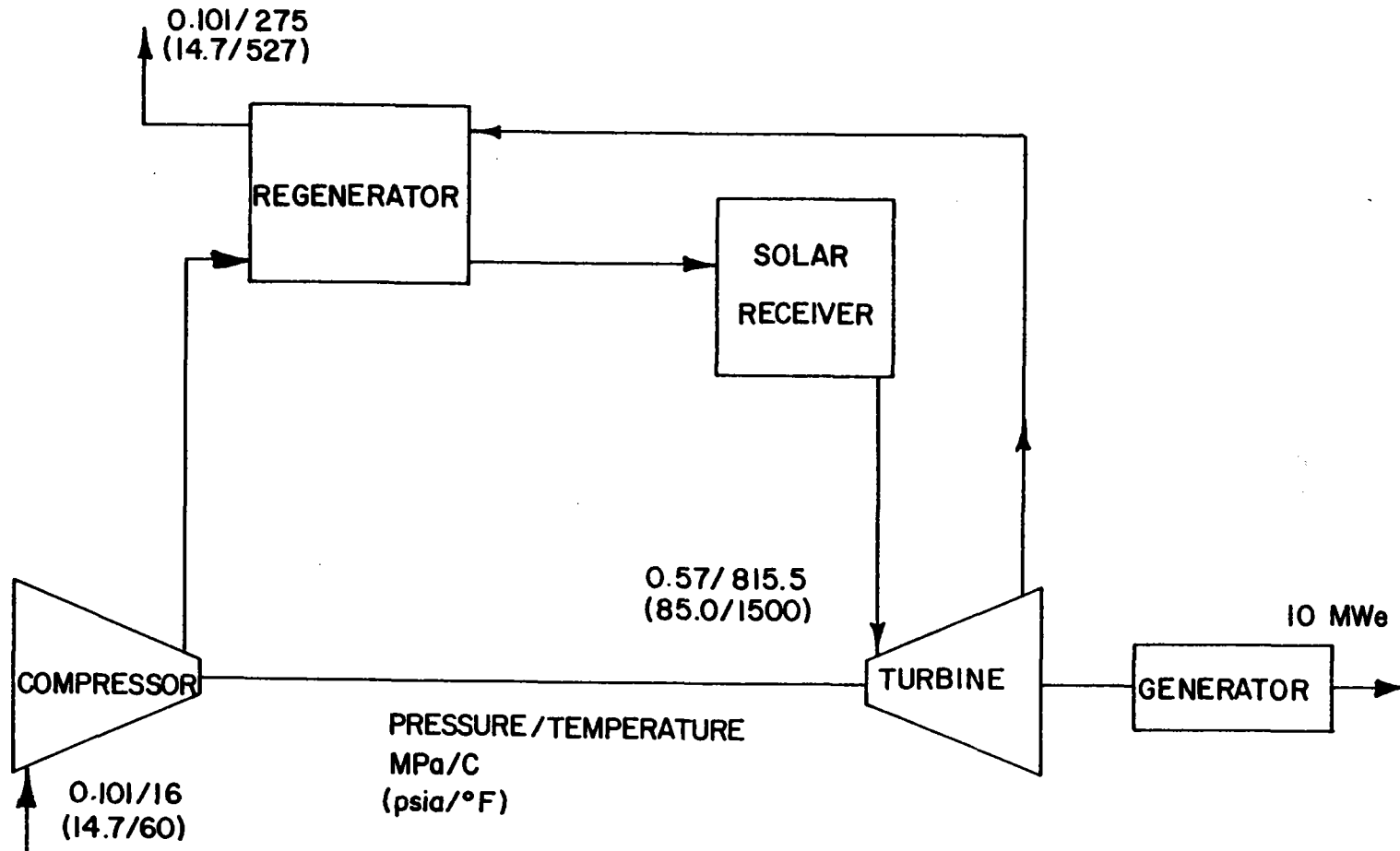


Figure 3.1 Regenerative Open Air Cycle Flow Diagram

FOSTER WHEELER DEVELOPMENT CORPORATION

REF.: 9-41-341106

DATE: September 15, 1978

for final heating. Instead, the air enters the solar receiver, where it is heated to a turbine-inlet temperature of 816°C (1500°F) and then expanded through a single-shaft, two-stage turbine. Air leaving the turbine at about 465°C (870°F) is subsequently cooled in the regenerator and exhausted to the atmosphere at approximately 275°C (525°F).

Section 4

DESCRIPTION OF THE PLANT

The plant design incorporates a conventional and commercially available open-cycle regenerative gas turbine as the prime mover. A high-temperature heat pipe receiver is used to heat the air to the high temperature required for efficient turbine operation. The gas-turbine generator unit and the solar receiver are both located at the top of a steel tower surrounded by an array of suntracking reflecting mirrors (heliostats).

4.1 COLLECTOR SUBSYSTEM

The collector subsystem is based on the heliostat field designed by Martin Marietta Corporation for their water/steam pilot plant.⁵ It is a north field arrangement with focusing heliostats symmetrically distributed about a north-south line from the tower, which is erected at the south edge of the collector field. The north field geometry provides the maximum optical collector efficiency. The focused heliostats enable the use of a smaller aperture for the cavity receiver, thus minimizing receiver losses. Each heliostat carried 41 m^2 (441 ft^2) of reflective surface.

As explained in Section 5.1, the required input energy to the receiver ranged from 30 to 34 MWt. Consequently, the number of heliostats required ranges from 1164 to 1344. They are laid out in 29 to 35 rows, as shown in the plot plan in Figure 4.1. Table 4.1 presents the heliostat field data.

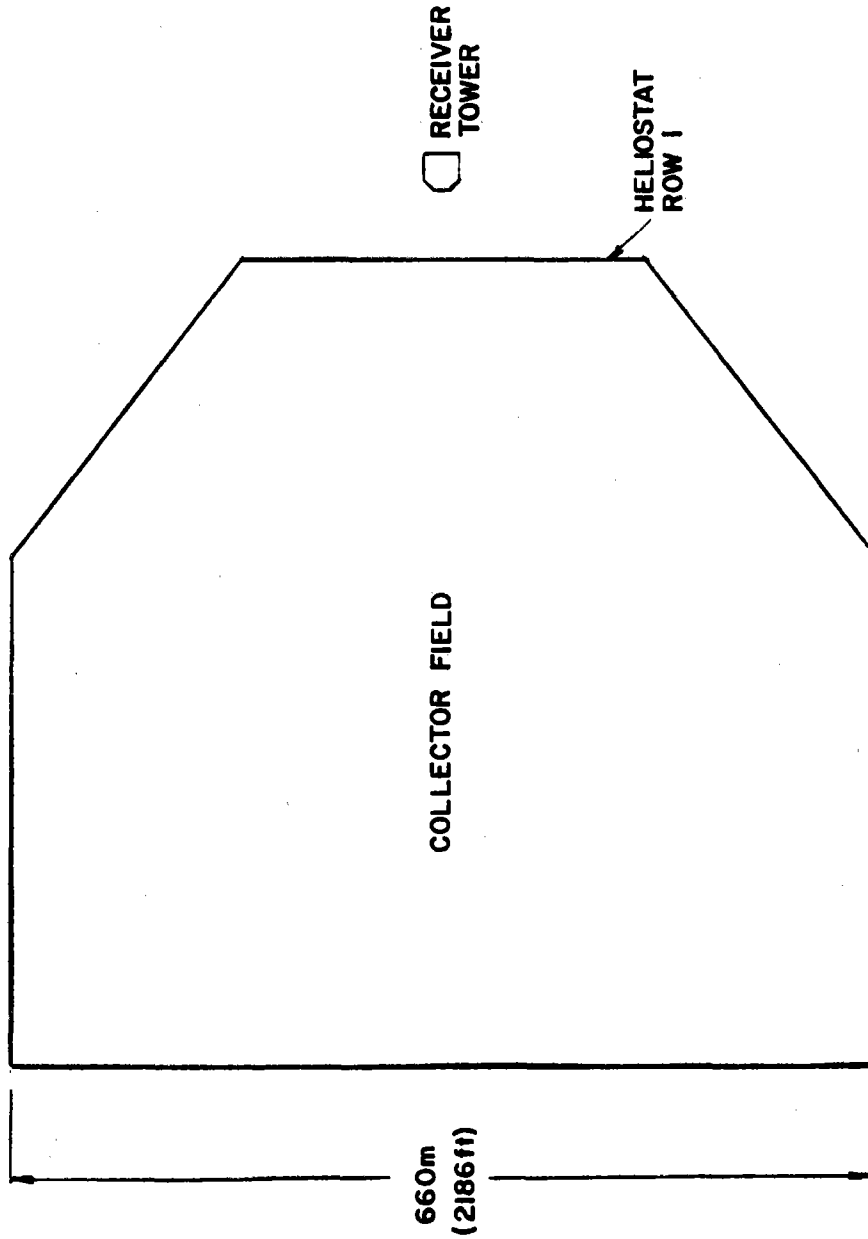


Figure 4.1 Plot Plan of Collector Field

Table 4.1 Heliostat Field Data

Number of heliostats	1164 to 1344
Number of rows	29 to 35
Distance from tower to first row, m (ft)	64 (210)
Distance from tower to last row, m (ft)	435 to 509 (1429 to 1669)
Field area, km ² (mi ²)	0.213 to 0.262 (0.082 to 0.140)
Reflecting surface per heliostat, m ² (ft ²) . . .	40.97 (441)

4.2 RECEIVER SUBSYSTEM

The receiver subsystem includes all components necessary to absorb the incident thermal energy from the heliostat field. The receiver conceptual design study addressed questions of technical and economical feasibility, such as cost, weight, size, surface requirements, materials, thermal efficiency (heat losses), air pressure drop, design complexity, operation and control, thermal transients, maintenance, and installation.

The basic approach to the design of the solar receiver subsystem was to make maximum use of existing design and fabrication technology. Preliminary design and cost studies were made to establish a feasible and economical receiver. These studies drew somewhat on the technical design data system cost analysis made by the three teams designing a water/steam solar pilot plant.^{2,6,7}

A variety of alternative receiver configurations were considered for this solar power plant in the earlier part of the project. During that preliminary evaluation, no specific heat-flux profiles were available. Consequently, reasonable values for peak and average heat fluxes were selected based on

previous central receiver studies performed for the water/steam solar pilot plants.

After the initial screening process, preliminary design of the three most promising candidates were developed. These candidates included one open (exposed) cylindrical configuration, one cavity cylindrical configuration, and one box configuration.⁸ Heat-loss calculations showed that an exposed receiver operating at the high outlet-gas temperature of 816°C (1500°F) chosen for the system gave prohibitive heat losses. This factor resulted in the adoption of a cavity-receiver configuration that provides maximum receiver efficiency. Further evaluation based on thermal/hydraulic, structural, and cost analyses led to the panel configuration shown schematically in Figure 4.2 and in detail in Drawing RD-780-11 (Appendix A). The chosen configuration provides:

- Maximum receiver efficiency by minimizing heat losses caused by reradiation, reflection, and convection
- Minimum pressure drop between compressor and turbine
- Maximum use of existing hardware and manufacturing techniques
- Modular design that enhances reliability, flexibility, and maintenance, since each panel is designed to be removable as a unit should replacement be necessary
- Optimum performance, since the airflow to each panel can be made proportional to the energy received by each panel
- Minimum cost.

The incident solar radiation from the heliostat field enters the cavity through an octagonal aperture. The requirement of a high receiver efficiency necessitates that the receiver aperture be large enough to collect a high

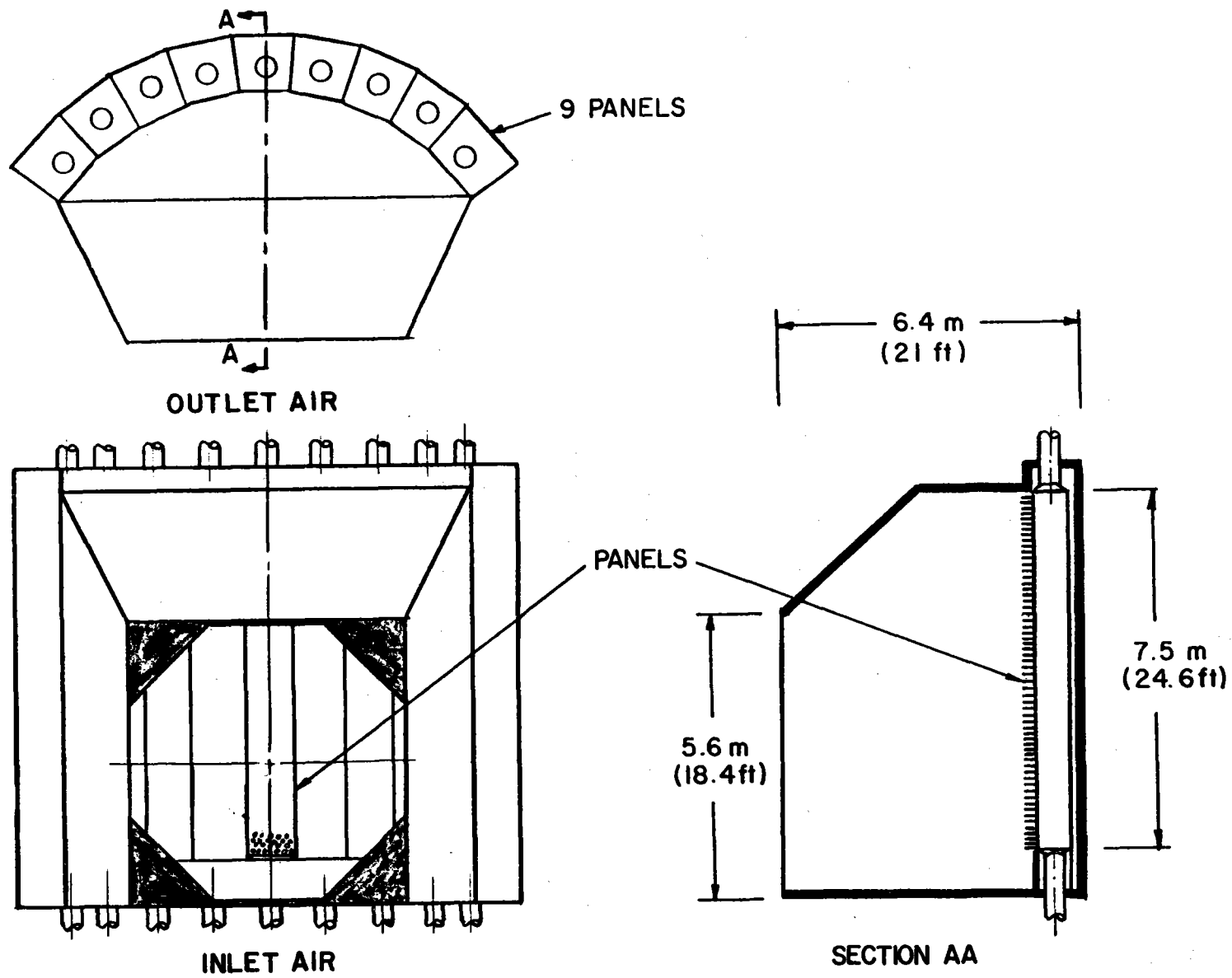


Figure 4.2 Cavity Receiver Configuration

percentage of the solar flux, yet small enough to prevent excessive heat losses by reradiation and reflection. To accomplish this, an octagonal receiver aperture was selected. By using an octagonal aperture, the stray or spillover heat-flux loss increases slightly, but the reduction in heat losses from the cavity more than compensates for this stray-loss increase.

The internal energy-absorbing surfaces that form the back of the receiver consist of nine panels, each 7.5 m (24.6 ft) high by 1.0 m (3.3 ft) wide, as shown schematically in Figure 4.3 and in detail in Drawing RD-780-12 (Appendix A). Four panels are 0.9 m (2.9 ft) deep, three are 0.8 m (2.6 ft) deep, and two are 0.6 m (2.16 ft) deep. The depth of each panel is a function of the amount of air passing through it, which in turn is proportional to the amount of heat flux impinging upon and being absorbed by the panel. Panel depth is such that each panel has approximately the same pressure drop. The average panel weight is approximately 10,000 kg (22,000 lb). As shown in Figure 4.3 and in Drawing RD-780-12, each panel consists of 637 sodium-filled heat pipes, inlet and outlet plenums, insulation, and support structure.

A simplified schematic of a typical heat pipe is shown in Figure 4.4. The heat pipes, 60-mm (2.375-in.) O.D., are installed in an 11.5-mm (4.5-in.) triangular-pitch pattern, as shown in Figure 4.5, and are attached to the front and back plates of the panel, as shown in Figure 4.6, so that they can be removed from the back of the panel in case of failure. The evaporator surfaces of the heat pipes, which protrude about 0.3 m (1 ft) from the front panel plate, absorb the incident high solar heat flux. The heat pipes then isothermally transport the energy to the finned condenser section. Further details of

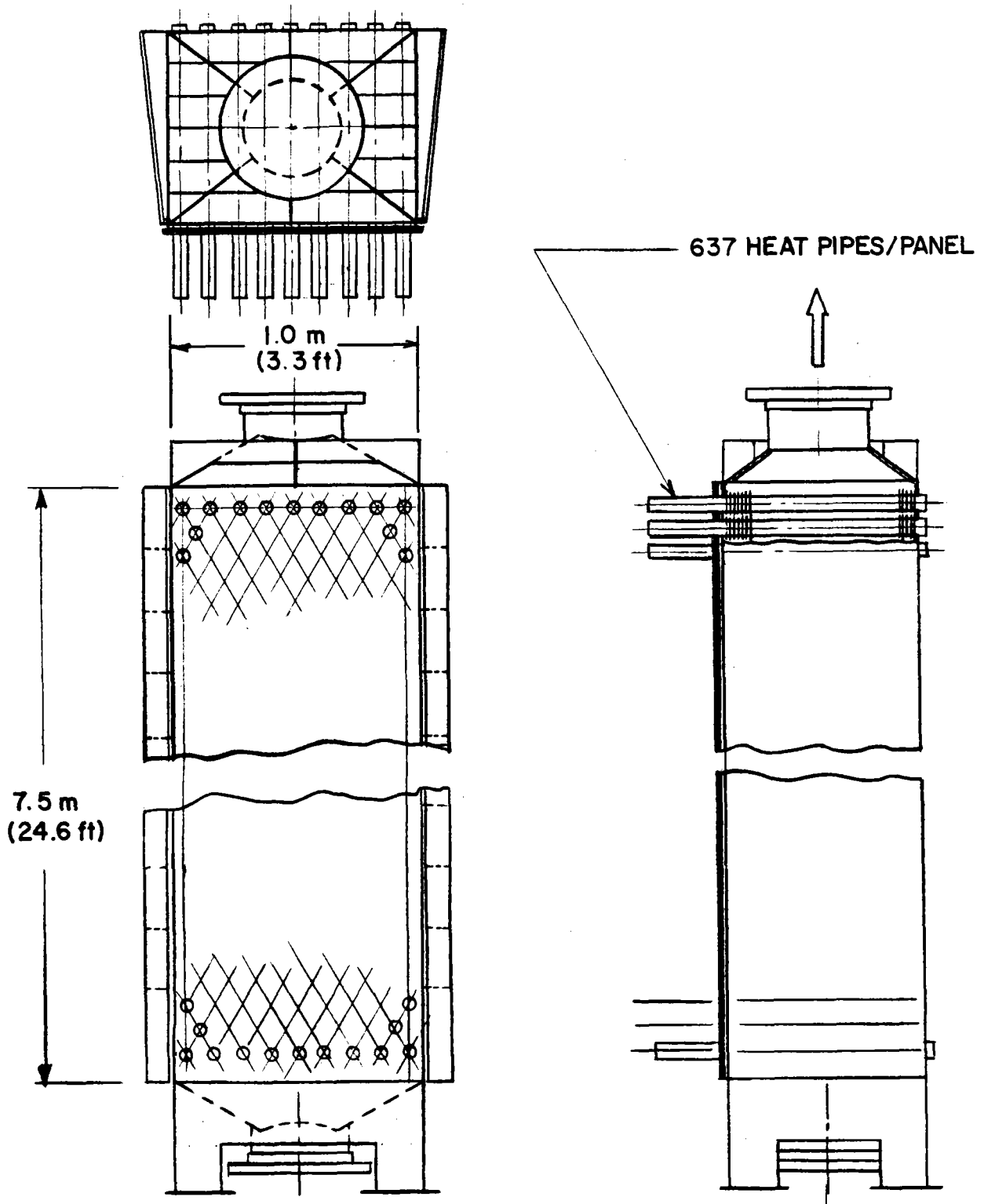


Figure 4.3 Panel Configuration

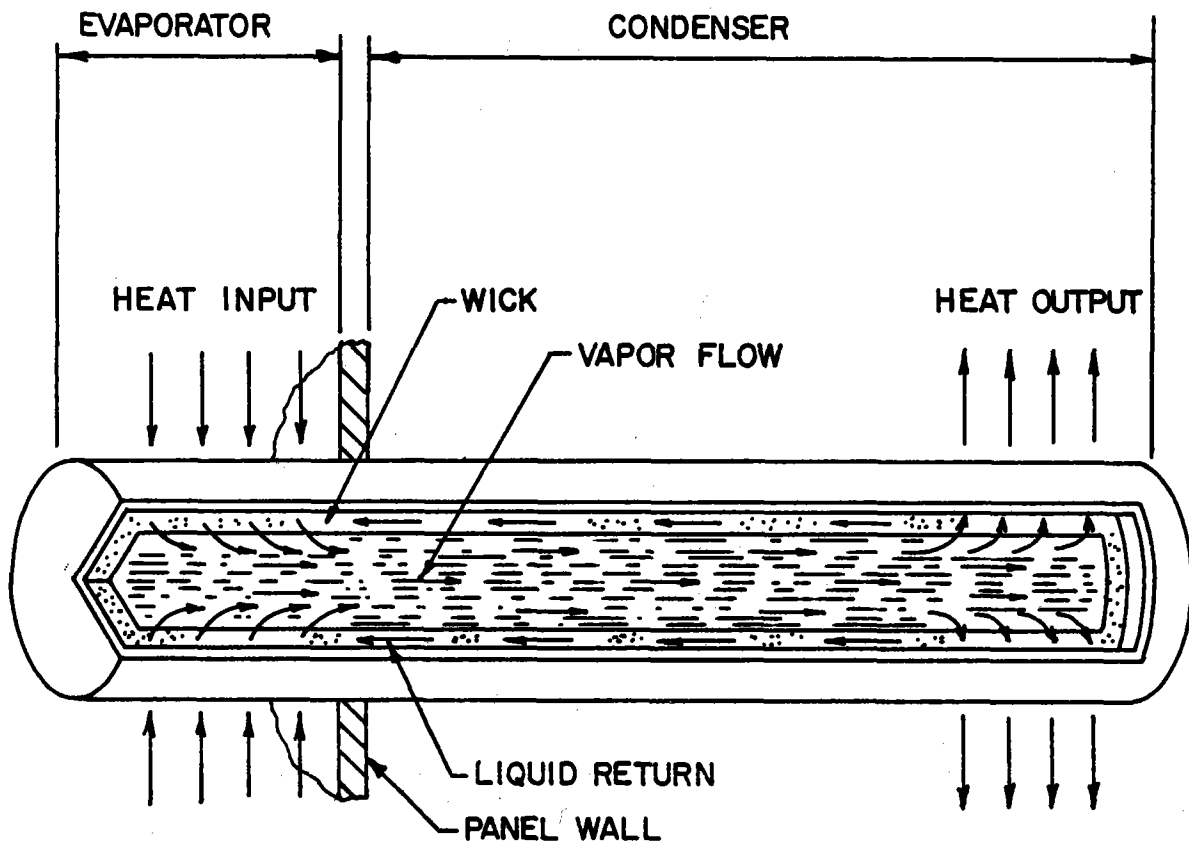


Figure 4.4 Schematic of Heat Pipe

the heat pipes will be given by Dynatherm in their final report. Compressed air is introduced at the bottom of the panels and is gradually heated by thermal contact with the fins as it passes upward across the finned condenser section of the heat pipes. The compressed air also receives some heat from contact with the insulated front wall of the panel.

The purpose of the 0.3-m (12-in.) protruding section of the heat pipes is twofold: It provides enough area to keep the heat flux in the evaporator section below design limits, and it shades the front-panel wall area between

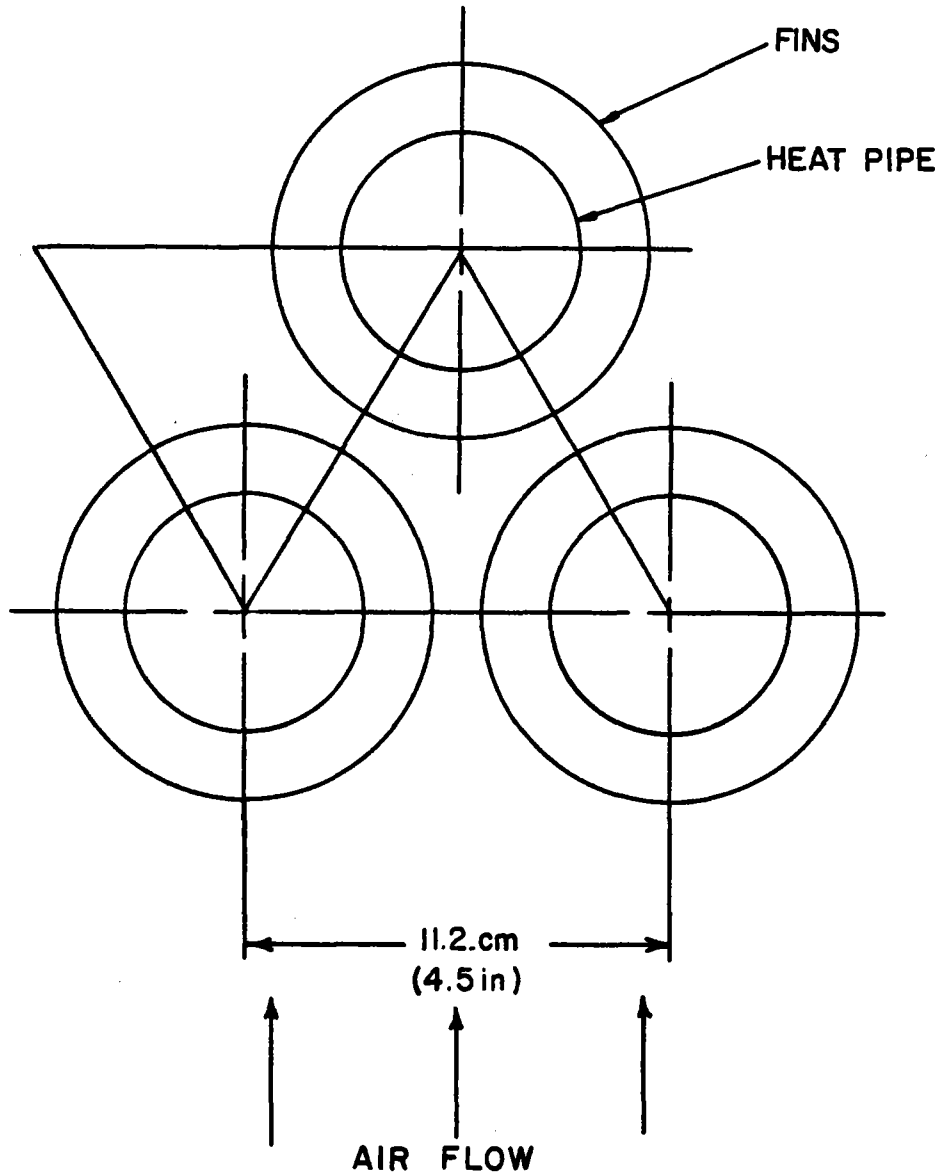


Figure 4.5 Typical Heat Pipe Layout

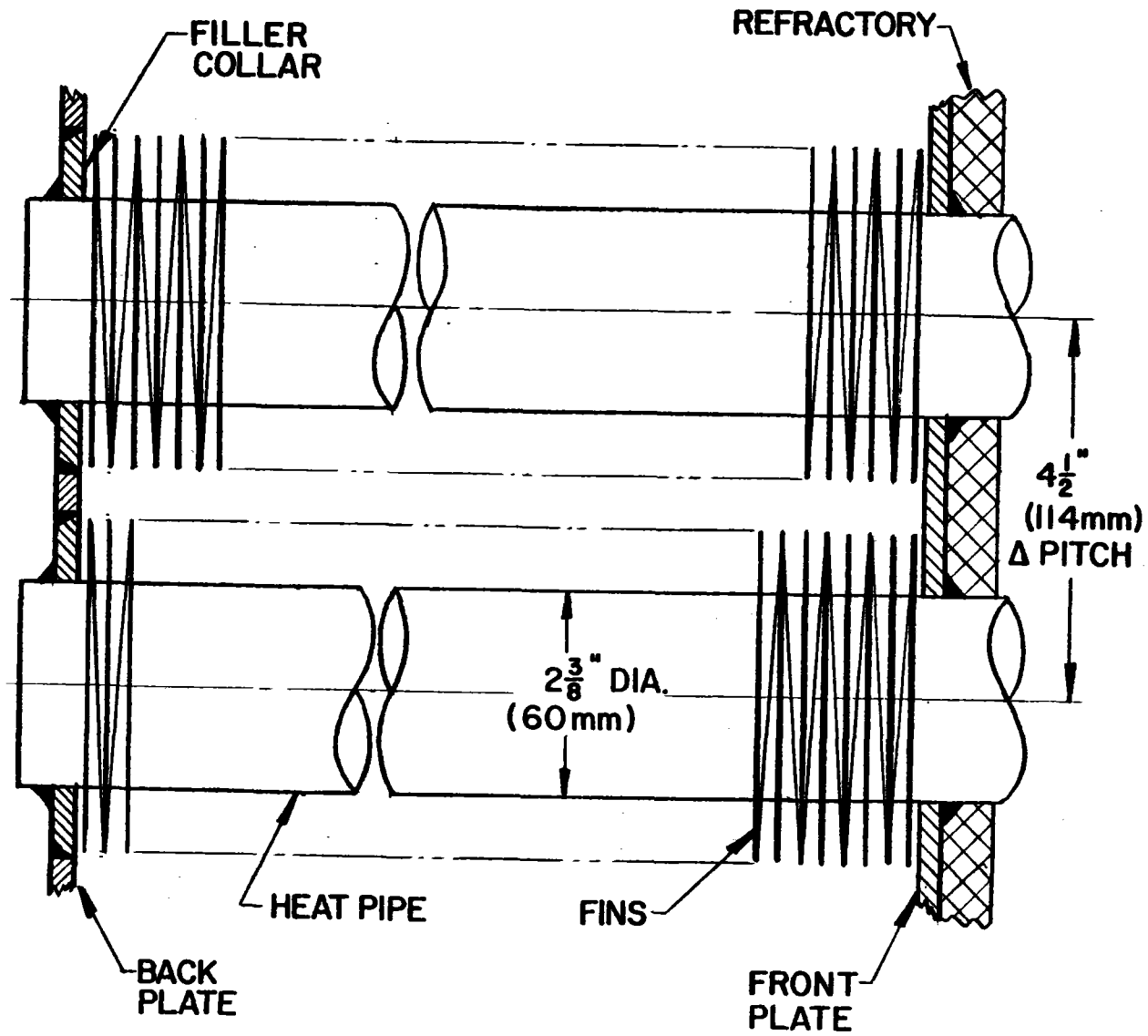


Figure 4.6 Schematic of Heat Pipe Installation

heat pipes from direct exposure to the high solar heat flux. As additional protection, the area between heat pipes is faced with Fiberfrax™ ceramic fiber that overlaps along the entire length where the panels join each other so that no heat flux will be allowed to leak through the spaces between the panels. The Fiberfrax is a light, fluffy refractory fiber made by Carborundum Company capable of withstanding continuous temperatures up to 1427°C (2600°F).

The inner surfaces of the cavity that are not panels are faced with either steel coated with reflective material or refractory, depending on the intensity of incident solar flux on the particular surface. The outer surface of the cavity is encased in weatherproofed insulation covered by corrugated aluminum sheathing.

4.3 INTERCONNECTING PIPING

The compressed, preheated air from the regenerator must be directed to the solar receiver and then ducted into the turbine for expansion. The heat losses and pressure drop in the piping linking these components should be as low as possible, since they have a strong impact on cycle efficiency. Details of the interconnecting piping are shown in Drawing RD-780-13 (Appendix A).

The compressed, preheated air leaves the regenerator via two conventional 0.66-m (26-in.)-diameter carbon steel pipes, one attached to each regenerator discharge port. A 0.66-m (26-in.)-diameter inlet manifold distributes the air to each panel via butterfly control valves located at the bottom inlet of each panel.

A 0.76-m (30-in.)-diameter outlet manifold collects the hot air leaving the panels. Air from the outlet manifold goes to the turbine wrapper-connection flanges via two 0.76-m (30-in.)-diameter Incoloy 800 pipes. External insulation of all interconnecting piping reduces the exposed surface temperature to about 60°C (140°F). The longitudinal thermal growth of the panels and piping is absorbed by expansion bellows.

4.4 ELECTRIC POWER GENERATION SUBSYSTEM

The electric power generation subsystem consists of conventional utility-type power-plant components. The main criteria for component selection was that existing, proven equipment be used wherever possible and require as little modification as possible in order to minimize costs and avoid equipment delivery delays caused by lengthy and costly development programs. Another consideration was that the turbomachinery be capable of withstanding daily start-up and shut-down cycles over the 30-year plant operating design life. These conditions translate into a 13,000-cycle life design requirement. Maximum use of existing technology and equipment is desirable so that the gas solar system can have the greatest application potential in the relatively near future.

Contact with major turbine manufacturers was made, and several turbine configurations were evaluated. The evaluation criteria included consideration of near-term, utility-type commercial operation, complexity of modifications required, efficiency, size, and weight. Based on these considerations, the General Electric (GE) gas turbine-generator package G3132R regenerative-cycle, two-shaft heavy-duty gas turbine was selected for the pilot-plant application.

Its basic cross-section configuration is shown in Figure 4.7. It has a gross weight of 69,000 kg (152,000 lb).

The nominal rated capacity of the GE Model G3132R turbine-generator is 10.4 MWe. Actual output will depend on ambient-air temperature and turbine-inlet temperature. The quoted rated capacity assumes 15°C (59°F) and 0.10 MPa-absolute (14.7 lb/in²a) ambient-air temperature and pressure respectively.

Preliminary talks with GE gas-turbine technical personnel indicate that because the turbine subsystem is not subjected to unusual operating conditions, the standard commercial design equipment can be used with small modifications to some components, such as the combustor wrapper and compressor discharge casing. Modifications to the compressor-gas turbine interface where the combustor system is located in the current GE gas-turbine arrangement will be required, since the combustor would be removed from the turbine frame. The relatively high temperature--816°C (1500°F)--of the hot air returning to the gas turbine from the solar receiver exceeds current design limits used in the standard turbine-inlet wrapper-connection flange and will require special insulation and some materials substitution, and probably a reconfiguration of the hot-gas inlet-ducting arrangement. Preliminary discussions with GE technical personnel indicate that such modifications are feasible.

With the exception of the turbine, which requires minor modification as described above, all the equipment is composed of conventional off-the-shelf items. The generator is a 1200-r/min, 4160-V, 3-phase, 60-Hz air-cooled machine rated at 14,000 kVA at 0.85-capacity factor. It weighs 59,550 kg (131,000 lb).

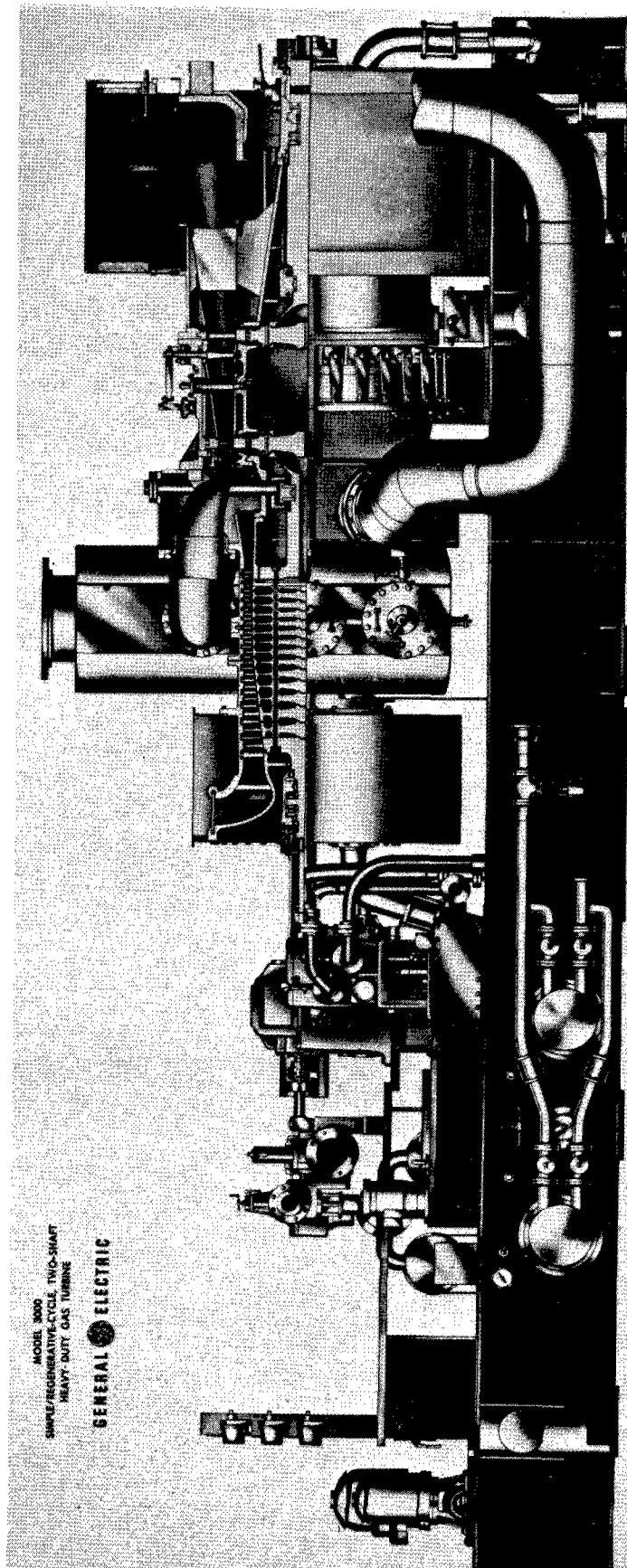


Figure 4.7 Gas Turbine Cross Section

The regenerator, which comes with the G3132R gas turbine-generator package, is the Harrison Regenerator Model TR-105 manufactured by the Harrison Radiator Division of General Motors Corporation. This regenerator is shipped in sections, thus facilitating installation on top of the tower. Its overall weight is 49,000 kg (108,000 lb).

The G3132R turbine-generator has its own control system that must be integrated through the master control center with the collector field system. Details of the instrumentation and control remain to be determined. To protect the gas turbine from extreme temperature variations, the inlet air should maintain a relatively constant temperature at the gas-turbine inlet. In the event of passing clouds, the control system will attempt to maintain outlet temperature by throttling flow rate. However, a problem exists in the event of a sudden load interruption, e.g., the main generator breakers open. In that case there would almost certainly be enough thermal inertia to overspeed the gas turbine, which could take place in a matter of seconds. Thus a sudden load interruption will require a fast-acting intercept-release valve installed in the duct prior to the turbine inlet to insulate the gas turbine and vent the hot air to the atmosphere in the event of a system trip.

4.5 TOWER SUBSYSTEM

The central receiver tower supports the cavity receiver and the gas turbine-generator set. They are all mounted on a structural steel support platform on top of the tower in order to minimize the airflow path among compressor, regenerator, receiver, and turbine and thus reduce the thermal and pressure losses and piping costs. This is particularly important because

large-diameter pipes are needed between the turbine regenerator and receiver to transport large volumes of air.

A plant view of the receiver and components is shown schematically in Figure 4.8 and in further detail in Drawing RD-780-13. Details of the supporting platform are given in Drawing RD-780-14. The location of the components and receiver in the supporting platform enables very uniform loading of the tower structure and provides easy personnel access to the receiver, turbine-generator set, and piping. The estimated weights for each component are given in Table 4.2. The overall weight on top of the tower is approximately 396 tons.

Table 4.2 Estimated Component Weight

<u>Component</u>	<u>Estimated Weight</u>	
	<u>lb</u>	<u>kg</u>
Receiver	238,250	108,295
Platform and support steel	81,500	37,045
Piping	20,700	9,409
Sheathing and insulation	60,700	27,591
Gas turbine	152,000	69,091
Electric generator	131,000	59,545
Regenerator	<u>108,000</u>	<u>49,091</u>
TOTAL	792,150	360,067

The structural-steel tower is similar in design to the one designed by McDonnell Douglas Astronautics Company for the water/steam solar pilot plant.⁹

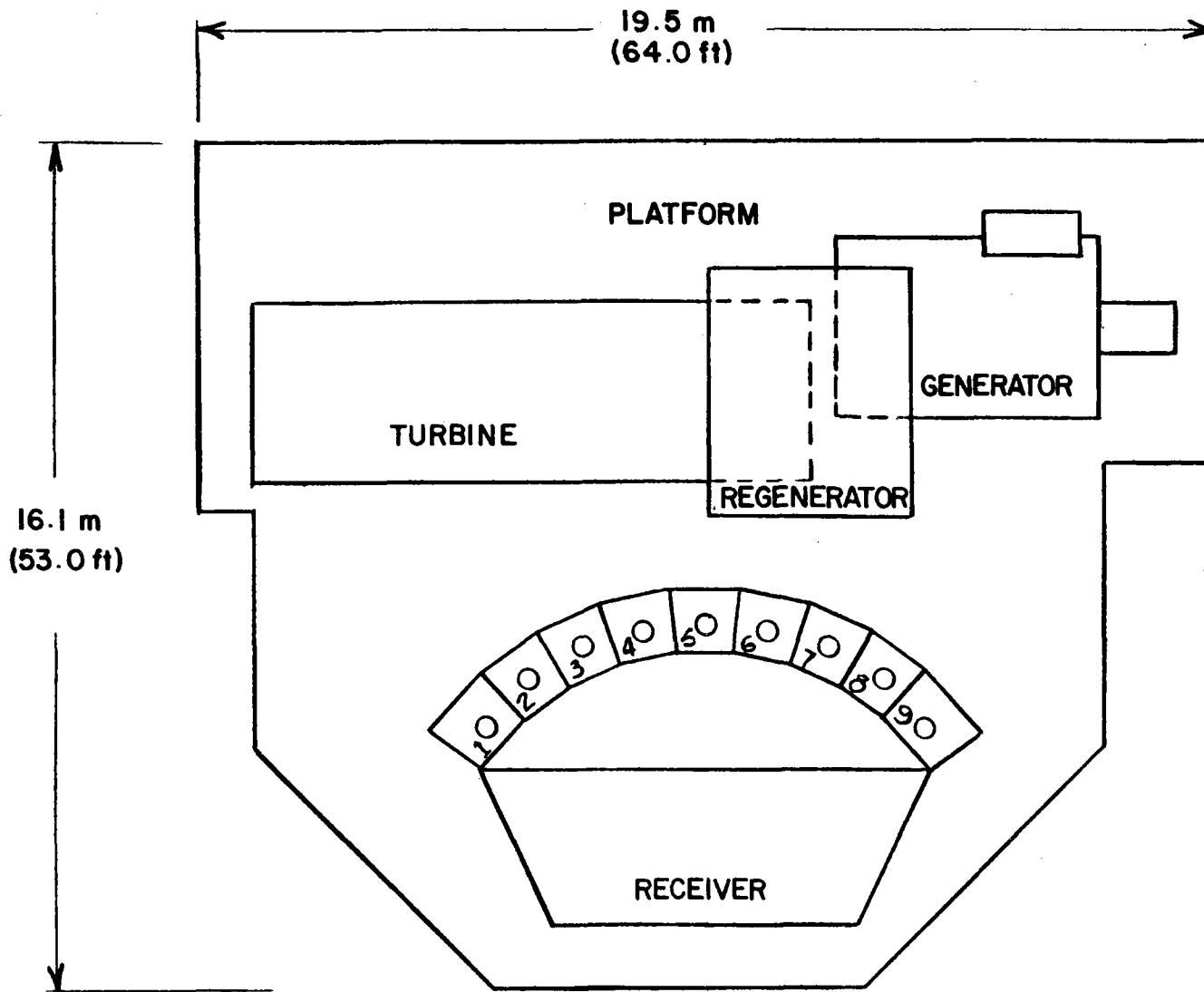


Figure 4.8 Plan View of Platform Showing Component Location

FOSTER WHEELER DEVELOPMENT CORPORATION

REF.: 9-41-341106

DATE: September 15, 1978

The tower, which is approximately 90 m (295 ft) high, provides for a personnel elevator and stairway and a generator bus-bar cable leading to the electric power substation located at the base of the tower. The center of the receiver aperture is 2.8 m (9.2 ft) above the tower platform, and the receiver is about 9.5 m (31.1 ft) high, giving an overall height of approximately 100 m (328 ft).

Section 5

PERFORMANCE ANALYSIS

5.1 PLANT ENERGY CHAIN

The plant energy flow diagram is shown in Figure 5.1. The upper and lower bounds of the plant-energy-chain performance are shown on an itemized basis in Figure 5.2. The stair-step chain format shows the power flow through the plant starting with the amount of incident solar power to the heliostat field. The chain accounts for all losses resulting in the required 10 MW of net electric power being produced by the generator. The main losses are discussed below:

- Balance of plant requirements were estimated at 0.25 MWe.
- Cycle efficiency, as indicated in Table 3.1, ranges from 33 to 38 percent, depending on the efficiency of the components--turbine, compressor, recuperator--chosen for the system.
- Heat losses by reradiation and convection for the cavity receiver were estimated using analytical methods and extrapolation of published data for similar cavity-type receivers. The results of this analysis indicate that the heat losses range from 3 to 4 MWt.
- Collector-system-performance losses were taken from Reference 5.

Starting with the required net electrical power output of 10 MW and combining the losses described above, the upper and lower bounds of the stair-step energy chain can be determined. The upper bound of the energy chain assumes a cycle efficiency of 33 percent and receiver heat losses of 4 MWt. The lower bound assumes a cycle efficiency of 38 percent and receiver heat losses of 3 MWt. The energy chain (Figure 5.2) shows that the required incident solar

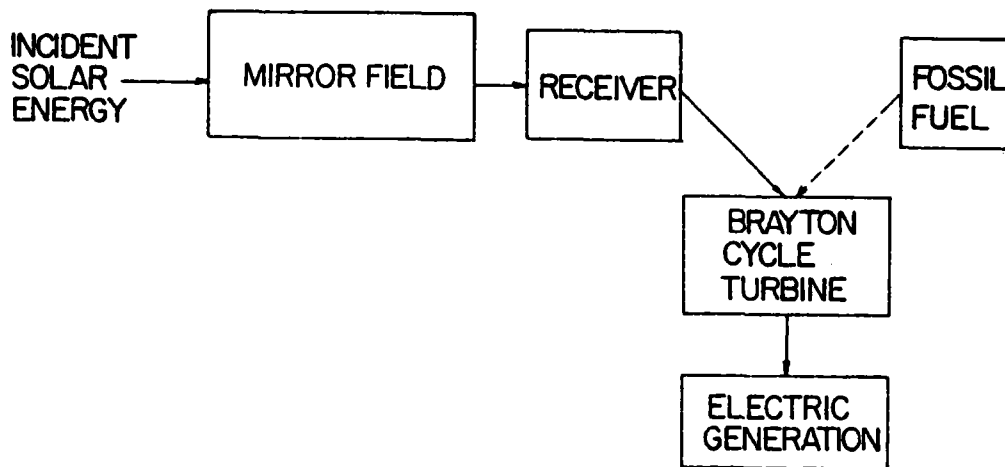


Figure 5.1 Plant Energy Flow Diagram

radiation delivered to the receiver aperture ranges from 30 to 34 MWt, thus the incident solar power to the heliostat field must be 45 to 52.3 MWt. Consequently, the overall system efficiency between the power incident to the heliostats and the net electrical power output ranges from 19.1 to 22.3 percent.

5.2 HEAT-FLUX PROFILES

To minimize the receiver surface area so that the receiver heat losses are reduced as much as possible, the heat flux incident upon the receiver must be maximized within the limits of receiver material capabilities, such as stress and fatigue life. These will be discussed in Section 6.

Because of the high heat-transfer capability of the heat pipes, the receiver is capable of accommodating the high heat flux resulting from a one-point aim strategy. Heat-flux maps that reflect the requirements of the lower bound of the energy chain (approximately 30 MWt into the cavity receiver) were provided by Dynatherm for the design-point conditions of 2 p.m. on summer

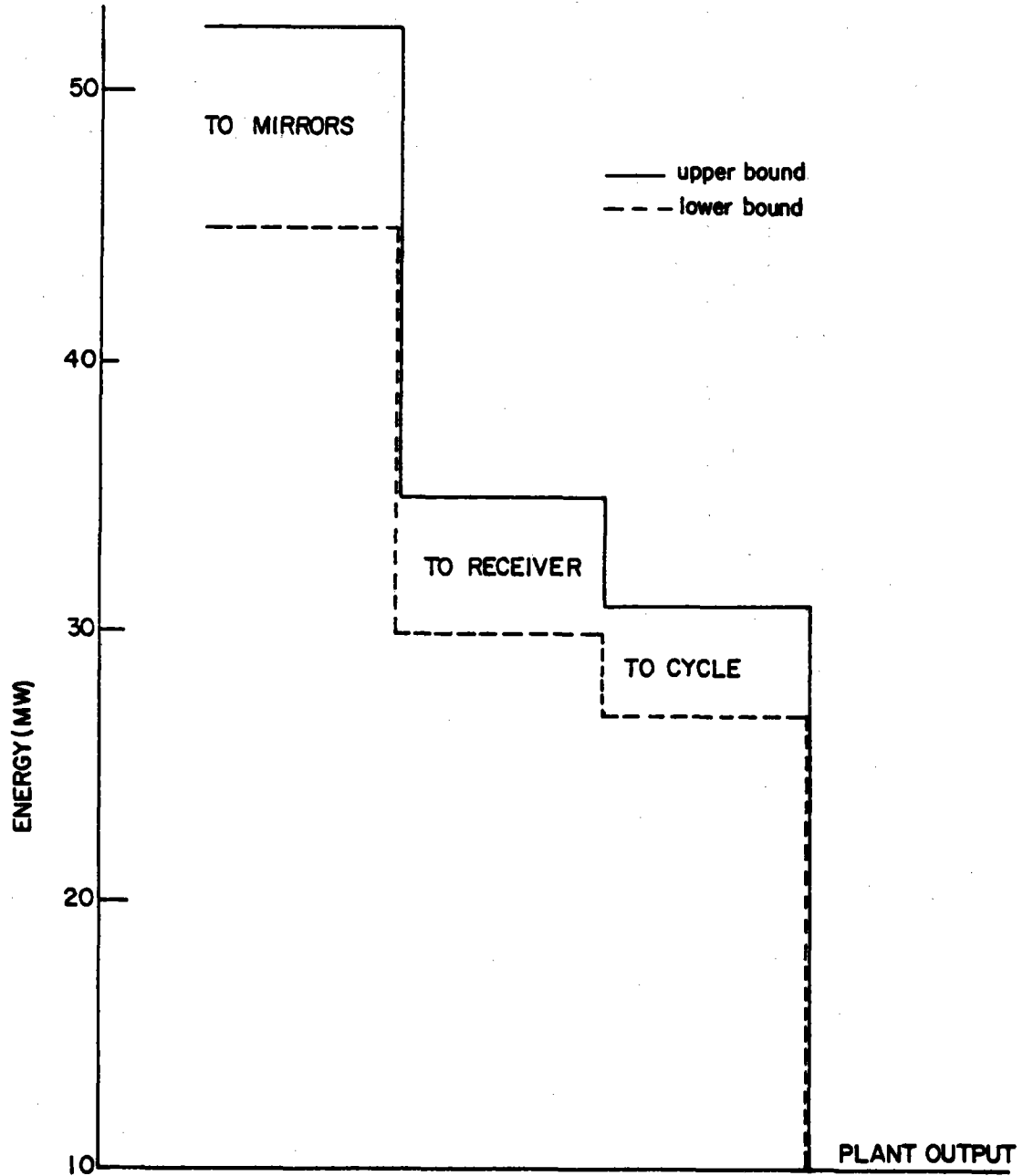


Figure 5.2 Plant Energy Chain

solstice. From these heat-flux maps, FWDC calculated the incident heat-flux density to each panel (Table 5.1). The corresponding heat-flux profiles are shown in Figure 5.3. Table 5.2 gives the incident average energy to each panel zone (10 zones per panel). The peak heat-flux density resulting on the receiver panels is approximately 1.16 MW/m^2 ($370,000 \text{ Btu/h}\cdot\text{ft}^2$), with an average heat-flux density of 0.45 MW/m^2 ($142,600 \text{ Btu/h}\cdot\text{ft}^2$).

A similar analysis was made to reflect the upper-bound requirements of the energy chain, namely 35 MWt into the cavity receiver. The results show a peak heat-flux density of 1.322 MW/m^2 ($428,500 \text{ Btu/h}\cdot\text{ft}^2$), with an average heat-flux density of 0.52 MW/m^2 ($165,000 \text{ Btu/h}\cdot\text{ft}^2$).

5.3 THERMAL/HYDRAULIC ANALYSIS

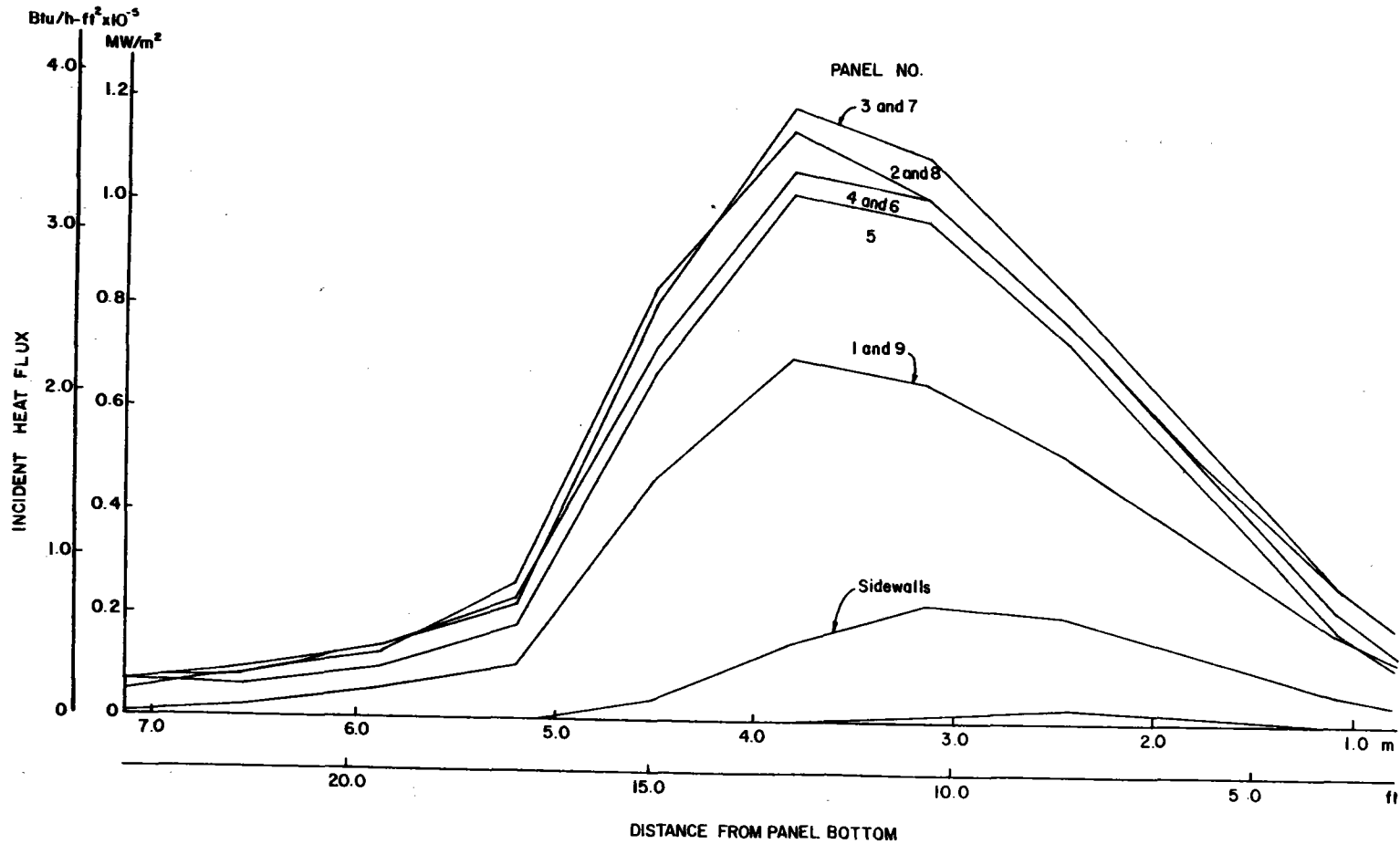
Figure 5.4 shows the airflow distribution to the panels, which is proportional to the solar power received by each panel. Once the mass flow was established, the depth of each panel was determined so that the pressure drop was approximately constant for all panels.

The heat-transfer coefficient between the air and the finned heat pipes was calculated using Foster Wheeler design manuals. The average, overall heat-transfer coefficient for the finned section of the heat pipes is $65 \text{ W/m}^2\cdot\text{°C}$ ($11.5 \text{ Btu/h}\cdot\text{ft}^2\cdot\text{°F}$), which assumes a sodium-condensing heat transfer coefficient of $28,333 \text{ W/m}^2\cdot\text{°C}$ ($5,000 \text{ Btu/h}\cdot\text{ft}^2\cdot\text{°F}$).¹⁰

The heat-transport requirements of the heat pipes at different locations along the panels are given in Table 5.3. These were calculated based on the

Table 5.1 Incident Heat-Flux Density to Panel Zones

Distance From Bottom of Panel (%)	Heat-Flux Density, MW/m ² (10 ³ Btu/h·ft ²)				
	Panel No.				
	5	4 and 6	3 and 7	2 and 8	1 and 9
90 - 100	0.0698 (22.126)	0.0711 (22.531)	0.0650 (20.601)	0.0422 (13.371)	0.0048 (1.522)
80 - 90	0.0655 (20.760)	0.0861 (27.283)	0.1000 (31.698)	0.0908 (28.786)	0.0262 (8.315)
70 - 80	0.1157 (36.671)	0.1633 (51.759)	0.1569 (49.746)	0.1501 (47.575)	0.0704 (22.307)
60 - 70	0.2646 (83.866)	0.3182 (100.865)	0.3172 (100.545)	0.3705 (117.432)	0.1601 (50.760)
50 - 60	0.9108 (288.684)	0.9570 (303.331)	1.0857 (344.120)	1.0890 (345.166)	0.7023 (222.589)
40 - 50	1.0180 (322.662)	1.0602 (336.037)	1.1589 (367.321)	1.0763 (341.140)	0.8750 (277.332)
30 - 40	0.8151 (258.351)	0.8573 (271.733)	0.9170 (290.665)	0.8612 (272.979)	0.7446 (236.013)
20 - 30	0.5257 (166.624)	0.5582 (176.915)	0.6122 (194.044)	0.5613 (177.914)	0.5036 (159.606)
10 - 20	0.2063 (65.388)	0.2454 (77.768)	0.2960 (93.819)	0.2893 (91.711)	0.2367 (75.001)
0 - 10	0.0106 (3.369)	0.0259 (8.195)	0.0674 (21.362)	0.0787 (24.938)	0.0479 (15.193)



5-6

Figure 5.3 Incident Heat Flux to Panels

Table 5.2 Incident Average Energy to Panel Zones

Distance From Bottom of Panel (%)	Average Energy, MW (10 ³ Btu/h)				
	Panel No.				
	5	4 and 6	3 and 7	2 and 8	1 and 9
90 - 100	0.0548 (17.378)	0.0558 (17.696)	0.0510 (16.180)	0.0331 (10.501)	0.0038 (1.195)
80 - 90	0.0514 (16.305)	0.0676 (21.428)	0.0785 (24.896)	0.0713 (22.608)	0.0206 (6.531)
70 - 80	0.0909 (28.802)	0.1283 (40.651)	0.1233 (39.070)	0.1179 (37.365)	0.0553 (17.520)
60 - 70	0.2078 (65.868)	0.2499 (79.219)	0.2491 (78.968)	0.2910 (92.231)	0.1258 (39.867)
50 - 60	0.7153 (226.732)	0.7516 (238.236)	0.8527 (270.271)	0.8553 (271.093)	0.5516 (174.821)
40 - 50	0.7995 (253.418)	0.8327 (263.923)	0.9102 (288.494)	0.8453 (267.931)	0.6872 (217.817)
30 - 40	0.6402 (202.909)	0.6733 (213.419)	0.7203 (228.288)	0.6764 (214.397)	0.5848 (185.364)
20 - 30	0.4129 (130.866)	0.4384 (138.949)	0.4808 (152.402)	0.4409 (139.733)	0.3955 (125.355)
10 - 20	0.1620 (51.355)	0.1927 (61.079)	0.2325 (73.685)	0.2273 (72.030)	0.1859 (58.929)
0 - 10	0.0083 (2.646)	0.0203 (6.436)	0.0529 (16.778)	0.0618 (19.586)	0.0376 (11.932)
Total Energy Per Panel	3.1433 (996.283)	3.4107 (1081.040)	3.7514 (1189.035)	3.6203 (1147.479)	2.6481 (839.334)
	10.48%	11.37%	12.50%	12.07%	8.83%

Note: Total energy to panel zones = 30.0042 MW/m² (9510.060 x 10³ Btu/h).

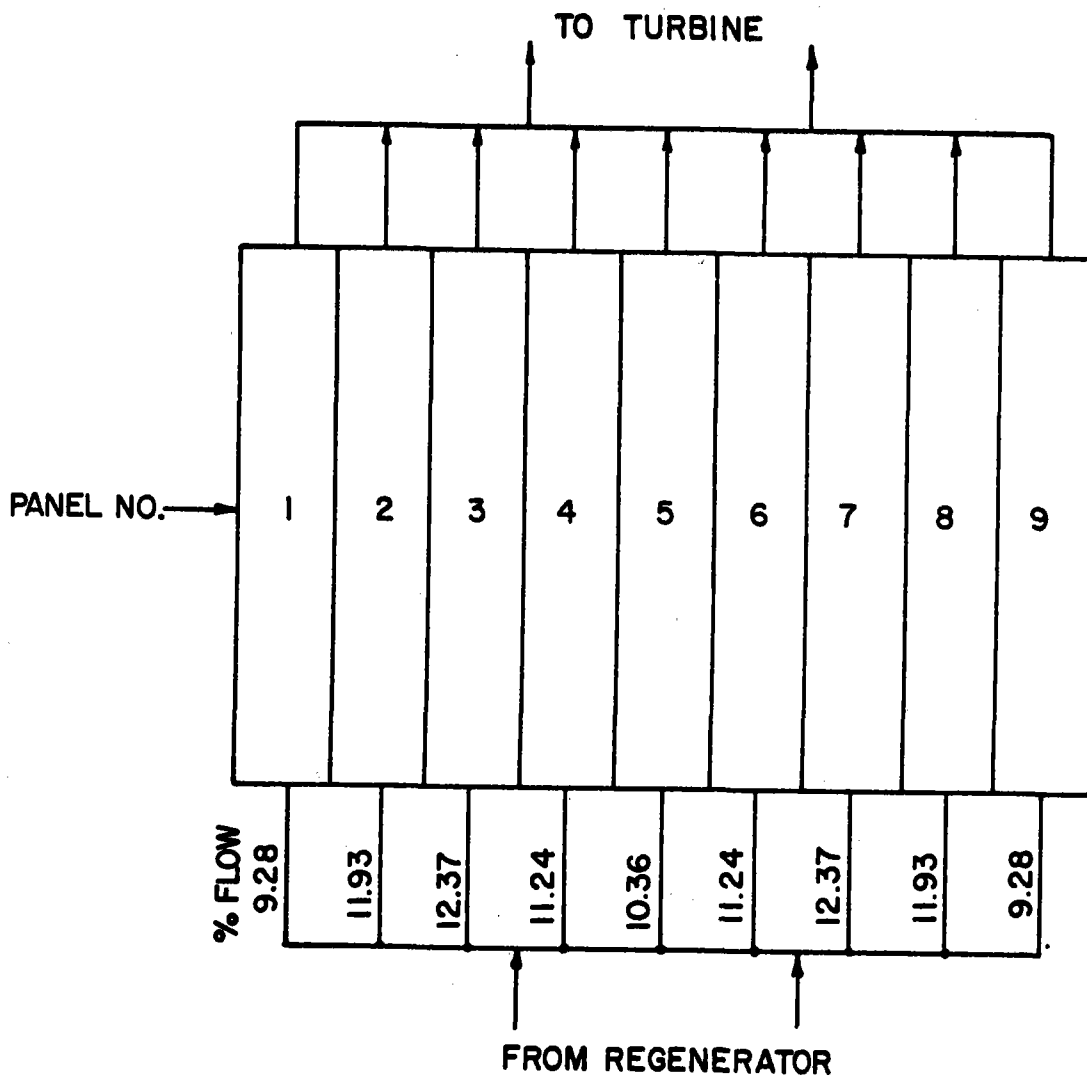


Figure 5.4 Air Flow Distribution

Table 5.3 Average Energy Transport Requirements

Distance From Bottom of Panel (%)	Average Energy (kW/heat pipe)				
	Panel No.				
	5	4 and 6	3 and 7	2 and 8	1 and 9
90 - 100	0.8	0.8	0.7	0.5	0.1
80 - 90	0.7	1.0	1.1	1.0	0.3
70 - 80	1.3	1.8	1.8	1.7	0.8
60 - 70	3.0	3.6	3.6	4.2	1.8
50 - 60	10.3	10.8	12.3	12.3	7.9
40 - 50	11.5	12.0	13.1	12.2	9.9
30 - 40	9.2	9.7	10.4	9.7	8.4
20 - 30	5.9	6.3	6.9	6.3	5.7
10 - 20	2.3	2.8	3.3	3.3	2.7
0 - 10	0.1	0.3	0.8	0.9	0.5

data given in Table 5.2. Air temperatures and the average heat pipe mean-wall temperature are given in Tables 5.4 and 5.5, which indicate that the peak average mean-wall temperature occurs slightly above the point of maximum heat-flux density. At this location the average mean-wall temperature is 841.1°C (1546°F), while at the exit, the average mean-wall temperature is 820.9°C (1509.7°F).

Table 5.4 Temperature of Air in the Panel

Distance From Bottom of Panel (%)	Air Temperature, °C (°F)				
	Panel No.				
	5	4 and 6	3 and 7	2 and 8	1 and 9
100	815.6 (1500.0)	815.6 (1500.0)	815.6 (1500.0)	815.6 (1500.0)	815.6 (1500.0)
90	809.1 (1488.3)	809.5 (1489.0)	810.5 (1490.9)	812.1 (1493.9)	815.0 (1499.0)
80	803.0 (1477.3)	802.1 (1475.7)	802.7 (1476.8)	804.8 (1480.6)	812.1 (1493.8)
70	792.2 (1457.9)	788.0 (1450.5)	790.4 (1454.8)	792.7 (1458.8)	804.3 (1479.8)
60	767.5 (1413.6)	760.7 (1401.3)	765.7 (1410.2)	762.7 (1404.9)	786.6 (1447.9)
50	682.7 (1260.8)	678.6 (1253.4)	680.9 (1257.7)	674.6 (1246.3)	709.0 (1308.2)
40	587.9 (1090.2)	587.6 (1089.6)	590.5 (1094.9)	587.6 (1089.7)	612.3 (1134.1)
30	511.9 (953.5)	514.0 (957.2)	518.9 (966.1)	517.9 (964.3)	529.9 (985.9)
20	463.0 (865.4)	466.1 (870.9)	471.1 (880.1)	472.5 (882.6)	474.2 (885.6)
10	443.8 (830.8)	445.0 (833.0)	448.0 (838.5)	449.1 (840.5)	448.1 (838.5)
0	442.8 (829.0)	442.8 (829.0)	442.8 (829.0)	442.8 (829.0)	442.8 (829.0)

Table 5.5 Average Condensing Section Heat Pipe Mean-Wall Temperature

Distance From Bottom of Panel (%)	Average Temperature, °C (°F)				
	Panel No.				
	5	4 and 6	3 and 7	2 and 8	1 and 9
90 - 100	820.8 (1509.4)	820.9 (1509.7)	820.0 (1508.0)	818.4 (1505.2)	815.9 (1500.6)
80 - 90	814.0 (1497.2)	816.0 (1500.8)	817.3 (1503.2)	818.3 (1505.0)	816.9 (1502.5)
70 - 80	811.7 (1493.1)	814.6 (1498.2)	813.5 (1496.3)	815.1 (1499.1)	817.3 (1503.1)
60 - 70	812.4 (1494.2)	812.6 (1494.6)	812.4 (1494.3)	818.1 (1504.6)	816.1 (1501.0)
50 - 60	837.4 (1539.3)	835.0 (1535.0)	841.1 (1546.0)	838.3 (1540.9)	838.5 (1541.3)
40 - 50	766.4 (1411.6)	766.4 (1411.6)	767.2 (1413.0)	755.2 (1391.3)	778.1 (1432.7)
30 - 40	661.4 (1222.5)	665.0 (1229.1)	664.9 (1228.9)	657.7 (1215.9)	677.1 (1250.8)
20 - 30	563.5 (1046.2)	568.5 (1055.4)	572.5 (1062.5)	567.2 (1053.0)	577.9 (1072.3)
10 - 20	484.6 (904.2)	491.6 (916.9)	498.7 (929.6)	499.4 (931.0)	498.5 (929.3)
0 - 10	444.9 (832.8)	447.8 (838.0)	454.5 (850.1)	456.7 (854.1)	453.2 (847.7)

Section 6

STRUCTURAL ANALYSES

Structural analyses of the receiver configuration, described in Section 4 and illustrated in Figures 4.2 and 4.3, are presented here. The analyses relate to the final selected concept and exclude the various alternate designs considered during the early phase of the program. These analyses were limited in scope because of the funding and time limitations. Only key loading conditions and simplified analytical models were used.

The receiver is a shielded cavity-type design consisting of nine panels. Each panel is formed from a rectangular shell with a number of sodium-filled heat pipes protruding through the front plate. The heat pipes also provide the support to the front and rear walls of the receiver shell. The analyses reported herein are divided into four subsections relating to:

- Receiver shell
- Heat pipes
- Piping
- Support platform.

A discussion of the loading conditions relevant to these components precedes the report on the analyses.

6.1 LOADING CONDITIONS

The receiver is subjected to the following types of loading conditions:

- Pressure loads

- Thermal loads during normal operation
- Pressure and thermal cyclic loads resulting from diurnal start-up and shutdowns and from cloud covers
- Dynamic loads (wind, earthquake, flow-induced vibration)
- Dead loads (self weight, snow, support reactions, etc.)

All these loads, however, are not equally significant to all receiver components. The loads used in the analysis of particular receiver components are described below. The effects of the remaining loads should be determined when detailed design of the receiver is performed.

- Receiver shell - Only an internal pressure load of 0.507 MPa (73.5 lb/in²g) was considered in the design of the receiver shell walls and the two heads. A design temperature of 443°C (829°F) was used for the inlet head, and a design temperature of 816°C (1500°F) was used for the outlet head and the receiver shell walls.
- Heat pipes - The ends of the heat pipes protrude through the receiver shell and are directly exposed to the solar radiation. Therefore, a thermal analysis of the heat pipes was done to determine the allowable heat fluxes. Only the cyclic thermal loads were considered in the analysis. A total of 13,000 cycles, corresponding to a 30-year lifetime, were used. The effects of cloud covers and pressure loading on fatigue life were not considered.
- Piping - An internal pressure load of 0.507 MPa (73.5 lb/in²g) was considered. Design temperatures of 443°C (829°F) and 816°C (1500°F) were used for the air inlet and outlet pipes respectively.
- Support platform - Only the dead loads were considered in the design of the support platform. Dynamic loads--wind and earthquake loads--should be considered in the final design of the support platform.

6.2 RECEIVER SHELL

6.2.1 Front, Side, and Rear Walls

The receiver shell, shown in Drawing RD-780-12 (Appendix A), consists of a front plate, a rear plate, and stiffened side walls. The heat pipes are

welded to both the front and rear plates and will act as supports for these plates. The front plate is protected from direct solar radiation by a 1-in.-thick refractory wall, as shown in Drawing RD-780-12.

All plates are designed for a 0.507 MPa (73.5 lb/in²g) lateral pressure. The design temperature of 816°C (1500°F) is used for the front and the rear plates. The thickness of the front and back plates is 6.35 mm (0.25 in.). The design temperature for the side walls is 443°C (829°F) at the inlet region and 816°C (1500°F) at the outlet region. The side walls are tapered I-sections formed by 9.525-mm (0.375-in.)-thick flanges (plates) and a 6.35-mm (0.25-in.)-thick web. Web spacing is also shown in Drawing RD-780-12. Stresses in the front and rear plates are presented in Tables 6.1 and 6.2. The secondary

Table 6.1 Stresses in Front Plate

Design Conditions: Internal pressure = 0.507 MPa (73.5 lb/in²g)
 Temperature = 816°C (1500°F)

Material: Inconel 601

Stress Category	Allowable Stress MPa (ksi)	Calculated Stress MPa (ksi)
Primary Membrane (P_m)	115.1 (16.7)	8.9 (1.3)
Primary Membrane + Bending ($P_m + P_b$)	172.4 (25)	41.4 (6)
Primary and Secondary ($P_m + P_b + Q$)	344.7 (50)	162.0 (23.5)

Table 6.2 Stresses in Rear Plate

Design Conditions: Internal pressure = 0.507 MPa (73.5 lb/in²g)
 Temperature = 816°C (1500°F)

Material: Inconel 601

Stress Category	Allowable Stress MPa (ksi)	Calculated Stress MPa (ksi)
Primary Membrane (P_m)	115.1 (16.7)	8.9 (1.3)
Primary Membrane + Bending ($P_m + P_b$)	172.4 (25)	41.4 (6)
Primary + Secondary ($P_m + P_b + Q$)	344.7 (50)	327.5 (47.5)

stresses in these tables are computed from the consideration of compatibility between the ends of both the front and rear plates and the side walls. Stresses in the side walls near the inlet and outlet regions are shown in Table 6.3.

Table 6.3 Stress in Side Panels

Design Conditions: Internal pressure = 0.507 (73.5 lb/in²g)
 Temperature = 443°C (829°F) - Inlet
 = 816°C (1500°F) - Outlet

Material: Inconel 601

Stress Category	Allowable Stress MPa (ksi)	Calculated Stress MPa (ksi)
At Inlet: Primary bending (P_b)	344.7 (50)	265.5 (37.2)
At Outlet: Primary bending (P_b)	172.3 (25)	115.1 (16.7)

The various types of stresses have been evaluated according to Section VIII-Division 2 of the ASME Boiler and Pressure Vessel Code.¹¹ The ideas of Code Case 1592¹², as modified for solar applications,¹³ are utilized for high-temperature service.

6.2.2 Inlet and Outlet Heads

Structural details of the inlet and outlet heads are shown in Drawing RD-780-12. The heads consist of a pyramidal shell formed by 9.525-mm (0.375-in.)-thick plates, which are supported at five intermediate locations by 9.525-mm (0.375-in.) stiffeners. The shell is designed for an internal pressure of 0.507 MPa (73.5 lb/in²g). Design temperatures are 443°C (829°F) for the inlet head and 816°C (1500°F) for the outlet head. Stresses in the inlet and outlet heads are shown in Tables 6.4 and 6.5 respectively. These stresses are evaluated according to the procedures given in Reference 11.

Table 6.4 Stresses in the Inlet Head

Design Conditions: Internal pressure = 0.507 MPa (73.5 lb/in²g)
Temperature = 443°C (829°F)

Material: Carbon Steel

Stress Category	Allowable Stress MPa (ksi)	Calculated Stress MPa (ksi)
Primary Membrane (P_m)	89.4 (12.98)	17.9 (22.6)
Primary Membrane + Bending ($P_m + P_b$)	149 (21.6)	100 (14.5)

Table 6.5 Stresses in Outlet Head

Design Conditions: Internal Pressure = 0.507 MPa (73.5 lb/in²g)
 Temperature = 816°C (1500°F)

Material: Incoloy 800

Stress Category	Allowable Stress MPa (ksi)	Calculated Stress MPa (ksi)
Primary Membrane (P_m)	68.9 (10)	17.9 (2.6)
Primary Membrane + Bending ($P_m + P_b$)	103.4 (15)	100 (14.5)

6.3 HEAT PIPES

6.3.1 Stress Analysis

The heat pipes are the only major receiver components exposed to direct solar radiation. A cyclic thermal analysis of the heat pipes was conducted to determine the allowable heat fluxes for various values of the sodium temperatures. The financial and time constraints did not permit a thorough creep-fatigue evaluation based on a detailed inelastic analysis. Therefore, a simplified inelastic analysis was performed,¹⁴ and approximate values of the allowable heat fluxes vs. sodium temperature were computed. These values are presented in Table 6.6. An axisymmetrical model was used in this analysis.

Two important pressure stresses were not considered in the above computations:

- External pressure of 0.507 MPa (73.5 lb/in²g), resulting in compressive hoop stresses of 5.72 MPa (830 lb/in²)

- Tensile axial stresses of 46.2 MPa (6.7 ksi) resulting from the end constraints of the heat pipes at the front and rear walls.

These pressure stresses may have an effect on the creep-fatigue life of the heat pipes; they may also cause ratcheting. Both of these effects must be evaluated in the detailed design of the system.

Table 6.6 Allowable Heat Fluxes for an Axisymmetrically Heated Inconel 601 Tube vs. Inner Fluid Temperature*

Sodium Temperature °C (°F)	Inside Tube Temperature °C (°F)	Outside Tube Temperature °C (°F)	Allowable Stress MPa (ksi)	Allowable Heat Flux MW/m ² (10 ³ Btu/h·ft ²)
482 (900)	538 (1000)	714 (1318)	345 (50)	1.47 (466.275)
543 (1010)	593 (1100)	739 (1363)	296 (43)	1.31 (416.710)
606 (1123)	649 (1200)	770 (1417)	241 (35)	1.11 (353.015)
667 (1232)	704 (1300)	813 (1494)	217 (31.5)	1.05 (332.150)
721 (1331)	760 (1400)	857 (1575)	201 (29.2)	1.02 (332.150)
777 (1431)	816 (1500)	909 (1669)	192 (27.8)	1.00 (316.235)
845 (1554)	871 (1600)	942 (1727)	143 (20.8)	0.81 (257.185)

*No pressure.

6.3.2 Evaluation of Dynatherm Heat Pipe Test

In one of the heat pipe tests performed at Dynatherm, a localized hot spot on the heat pipe was observed; cracking occurred near the outer periphery of the hot spot. A brief summary of an analysis of this test follows.

The test specimen and loading parameters are listed in Table 6.7. Since the pressure stresses would be very small, they were ignored in the analysis.

Table 6.7 Test Specimen and Loading Parameters

Tube material	Inconel 601
Tube O.D.	57.15 mm (2.25 in.)
Tube I.D.	52.5 mm (2.067 in.)
Liquid sodium temperature	771°C (1420°F)
Heat flux75 MW/m ² (~240,000 Btu/h·ft ²)
Film coefficient.	30 KW/m ² ·°C (~5000 Btu/h·ft ² ·°F)
Internal pressure	Varies from ~13.8 Pa (2 lb/in ²) at 973 K (1292°F) to ~68.9 Pa (10 lb/in ²) at 1123 K (1562°F)
Test duration	Approximately 2 to 3 weeks
Number of cycles.	150

Three sources were postulated as causing the thermal stresses (summarized in

Table 6.8):

- Through-the-thickness temperature gradient - From the heat flux, liquid sodium temperature, film coefficient, and tube geometry, the through-the-thickness temperature gradient and resultant thermal stresses were determined. A compressive stress of 120.6 MPa (17.5 ksi) was computed at the outside surface, whereas a tensile stress of the same magnitude occurred at the inside surface.¹⁵
- Local hot spot - The local hot spot was mathematically simulated by assuming a film coefficient of 18 kW/m²·°C (3000 Btu/h·ft²·°F) in that region. This made the hot spot about 20°C (36°F) hotter than the neighboring region. An elastic thermal analysis resulted in compressive stresses of about 27.6 MPa (4 ksi) within the hot spot, whereas tensile stresses were found to exist in the region outside the hot spot.¹⁵
- Axial temperature gradient - An axial temperature gradient was expected to occur near the end of the evaporator (end of the heating coil). For the purposes of this analysis, an axial temperature gradient of 10.9°C/mm (500°F/in.) was assumed. This would create almost no circumferential stress.

Table 6.8 Thermal Stresses in Heat Pipe Test Conducted at Dynatherm

Stress	Caused by Through-the-Thickness Temperature Gradient* MPa (ksi)		Caused by Local Hot Spot MPa (ksi)		Caused by Axial Temperature Gradient† MPa (ksi)	
	Inner Radius	Outer Radius	Within Hot Spot	Outside Hot Spot	Inner Radius	Outer Radius
Circumferential (σ_{θ})	120.6 (17.5)	-120.6 (-17.5)	-27.6 (-4)	<27.6 (4)	Negligible	Negligible
Axial (σ_x)	120.6 (17.5)	-120.6 (-17.5)	-27.6 (-4)	>27.6 (4)	-68.9 (-10)	68.9 (10)

*Evaporator region.

†End of evaporator.

The axial stresses developed are opposite in nature from those related to the through-the-thickness temperature gradient. A tensile stress of 68.9 MPa (10 ksi) at the outside surface and a compressive stress of the same magnitude occurred at the inside surface.¹⁵

Table 6.8 shows that the maximum tensile stress occurs in the axial direction just outside the hot spot (within the evaporator region), at the inside surface of the heat pipe. Therefore, cracking would be expected to occur in the circumferential direction at that location, which was indeed the case in the Dynatherm test.

A metallurgical analysis was made of the hot spots in a test sample provided by Dynatherm. The report is presented in Appendix B.

6.4 INLET AND OUTLET PIPES

The piping arrangement is shown in Drawing RD-780-13 (Appendix A). The inlet and outlet pipes are designed for a pressure of 0.507 MPa (73.5 lb/in²g).

Design temperatures are: 443°C (829°F) for the inlet pipes and 816°C (1500°F) for the outlet pipes. The dimensions shown in Drawing RD-780-13 (Appendix A) are based on primary hoop stress resulting from internal pressure. Stress concentration effects at the connection of the piping to the shell are not considered in the design. The stresses in inlet and outlet pipes are shown in Table 6.9.

Table 6.9 Stresses in Inlet and Outlet Pipes

Design Conditions: Internal pressure = 0.507 MPa (73.5 lb/in²)
 Temperature = 427°C (800°F) - Inlet
 = 816°C (1500°F) - Outlet

Material: Carbon Steel - Inlet
 Incoloy 800 - Outlet

Stress Category	Allowable Stress MPa (ksi)	Calculated Stress MPa (ksi)
Inlet Pipe: Primary membrane (P_m)	89.4 (12.96)	26.2 (3.8)
Outlet Pipe: Primary membrane (P_m)	103.4 (15)	30.3 (4.4)

6.5 SUPPORT PLATFORM

The support platform, shown in Drawing RD-780-14 (Appendix A), is designed for the weight loads only.¹⁶ The support configuration is based on the loading and support points of various equipment supplied by platform manufacturers. Specific dimensions of each component in the support platform are also shown in Drawing RD-780-14. The final design of the support platform must evaluate the earthquake loads.

Section 7

HYBRID OPERATION CONSIDERATIONS

As previously mentioned, the plant can be modified to allow hybrid operation where the turbine operates by solar energy alone, by combustion of fossil fuel alone, or by a combination of both, so that the power generation is not subject to fluctuations in insolation. The operating mode of the plant at a given time will depend on the insolation level and the grid demand. Energy storage for operation during periods of no insolation would be provided by simple on-site fuel storage. Thus, hybrid operation represents a practical alternative to the use of thermal storage.

The hybrid capability, unique to the open-cycle gas-turbine system, enables the solar plant to be a reliable source of electricity despite weather or time of day. Therefore, the potential for hybrid operation represents one of the main advantages of this type of solar power plant.

Figure 7.1 shows the system schematic of the hybrid concept. The parallel fossil combustor-solar receiver system is compatible with standard combustion systems, since it would inherently adjust airflow with fuel flow. The parallel arrangement also reduces system pressure losses because the total airflow does not pass through the fossil combustor and the solar receiver, as in a series arrangement. The external combustors used in the parallel arrangement further simplify combustor system design by relieving size constraints and providing an opportunity for ample mixing of the flow streams, thus helping to protect the turbine from hot spots and thermal shock.

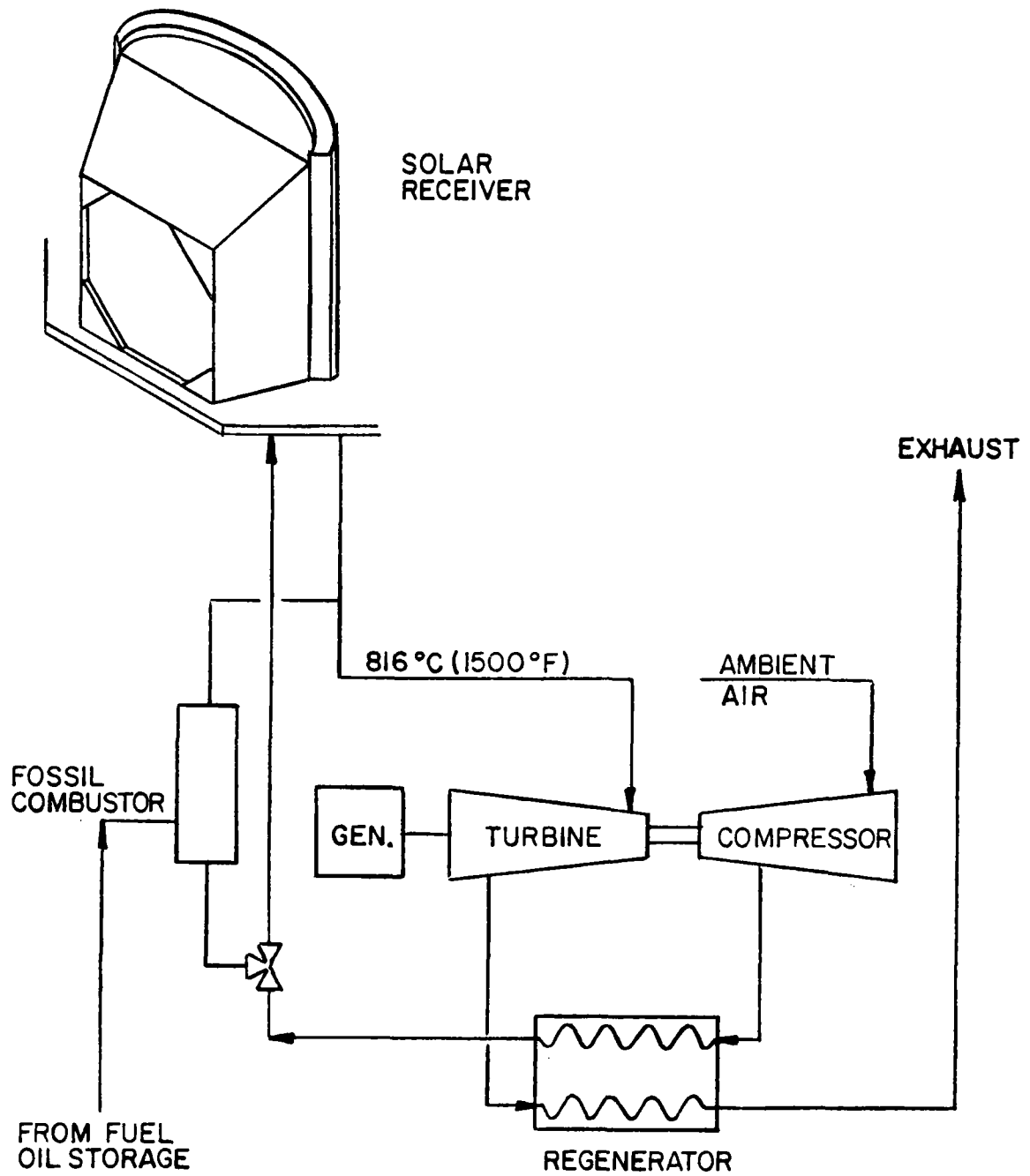


Figure 7.1 Hybrid, Open Brayton Cycle Central Receiver System

Conventional combustors have an extremely rapid response time, and they could be brought in line fast enough to compensate for a sudden reduction in insolation. There might be a temporary decrease in plant output, but a constant plant output could be sustained if all or part of the combustion system were operated at low load and if a cloud detection system were employed to provide advance warning of impending cloud cover. If the combustion system were kept operating at a reduced load, it could be used to increase the gas-turbine inlet temperature above that imposed by receiver-temperature limitations, thereby improving cycle efficiency and reducing plant cost per megawatt.

The use of a parallel combustor system offers several advantages, such as simplified system control, use of current design practice, and maximum utilization of available equipment and technology. Combustion system outlet temperatures, operating range, response times, and other factors can be controlled to assure stable output under abnormal operating conditions.

In the extreme case, the combustor system will be required to contribute from 0 to 100 percent of the plant rated output and to respond to very rapid fluctuations in solar input to the system resulting from changes in cloud cover. Since the solar plant has low thermal inertia, particularly with the gas-turbine system mounted on top of the tower, the combustor system must be able to respond to relatively large changes in power in relatively short periods of time. Therefore, the widely varying constant pressure airflow to the combustor may cause operational problems because of the reduced airflow velocities within the combustor at reduced flows. The wide range of combustor airflows may also result in relatively low combustor efficiency when the system is operating at very low

flows. However, if several combustors are used the airflow to an individual combustor could be adjusted by varying the number of on-line combustors with combustion system load. This would facilitate acceptable airflow distribution within each combustor and maintain high combustor efficiency, thereby minimizing fuel consumption during hot-standby operation. The multiple combustor system would also allow greater flexibility in controlling the airflows to the combustor system and solar receiver at any given operating conditions.

Thus, the hybrid system concept appears to present no major technological problems. Relatively standard design concepts and equipment can be used with only small modifications. Indeed, the advantages of hybrid operation far outweigh the additional cost of the system.

Section 8

PLANT CAPITAL COST

The capital costs presented in Table 8.1 were obtained by using vendor quotations wherever possible, Foster Wheeler cost-estimating experience, and cost figures for the water/steam plant with some adjustments to account for inflation and specific technical and hardware differences. The basic ground rules and assumptions were:

- No interest during construction
- Cost in mid-1978 dollars
- Free land and land rights as in the water/steam pilot plant
- Plant site at Barstow, California
- No development costs included.

An item-by-item discussion of the costs is provided below:

- Receiver and platform - This cost item covers the receiver unit, the platform, and all interconnecting piping with the turbine-generator set. It includes the labor and material required to design, fabricate, and support an acceptance test for up to 6 months. Material costs were based on actual vendor quotations and up-to-date catalog prices, heat pipe costs (\$2.4 million) were provided by Dynatherm, and receiver design and manufacture costs are based on Foster Wheeler experience. We assumed the receiver panels to be factory-assembled with on-site final receiver assembly.
- Transportation and installation - This cost item includes packing, transportation, and site-labor assembly and installation costs for the receiver, platform, and turbine-generator unit on top of the tower. Site labor costs are based on today's prevailing rates for the Barstow area.
- Tower assembly, foundation, and site preparation - These costs are based on the costs developed for the water/steam system. The costs

were adjusted to account for differences in tower height, weight on top of the tower, and inflation.

- Collector field - The cost of the collector field was assumed to be \$65/m².
- Buildings and facilities - This cost item includes all structures and facilities required for the plant, such as maintenance buildings and administrative buildings. It does not include a turbine-generator building, since these components will be located on top of the tower.
- Turbine-generator unit - This cost item includes the turbine, compressor, electric generator, regenerator, and instrumentation and control normally associated with a gas-turbine plant. It does not include the master control system of the plant.
- Master control - The details of the control system have not been developed. We assume that the cost will be the same as for the water/steam plant. This is a conservative assumption, since the master control system for the gas-solar plant is expected to be somewhat simpler.
- Miscellaneous - This cost item includes field communication, transportation and handling equipment, furnishing and fixtures, and maintenance and service equipment.

As shown in Table 8.1, the projected cost, in mid-1978 dollars, of the heat pipe central solar receiver gas-turbine plant ranges from \$1,947 to \$2,002/kW, depending on the assumed cycle efficiency.

Table 8.1 Capital Cost Estimates

<u>Item</u>	<u>\$ Million</u>
Receiver and platform	3.51
Transportation and installation	0.88
Tower assembly	1.50
Tower foundation and site preparation	0.54
Collector field (heliostats)	3.10 - 3.58
Buildings and facilities	0.50
Turbine-generator unit	2.97
Master control	2.24
Miscellaneous	<u>1.69</u>
Total direct costs	16.93 - 17.41
Contingency allowance and indirect costs (15%)	<u>2.54 - 2.61</u>
TOTAL CAPITAL COSTS	19.47 - 20.02

Section 9

CONCLUSIONS

Based on the results of this study, we can conclude that the open air Brayton cycle using a heat pipe central receiver is superior to a steam Rankine cycle using a water/steam receiver for the following reasons:

- Weight, heat losses, and cost are reduced through the utilization of higher heat-flux densities, resulting in reduced receiver size.
- Thermal efficiencies from 33 to 38 percent are possible as a result of higher cycle temperatures.
- Costs and pressure-drop losses are minimized because the turbine, generator, recuperator, and receiver are located at the top of the tower.
- Open gas cycles operate at lower pressure, are designed for cycling and quick start-ups, and do not require cooling water.
- The system may be modified to operate in a hybrid mode by burning fossil fuel during periods of no insolation, thereby increasing system availability and dependability.
- The high exhaust-air temperatures may be utilized in an organic bottoming cycle, further increasing the cycle efficiency up to 45 percent.
- Preliminary cost estimates indicate that capital costs per installed kilowatt are less than those for a water/steam system.
- The prototypical plant can be made truly representative of a commercial plant because only minor component development is required.

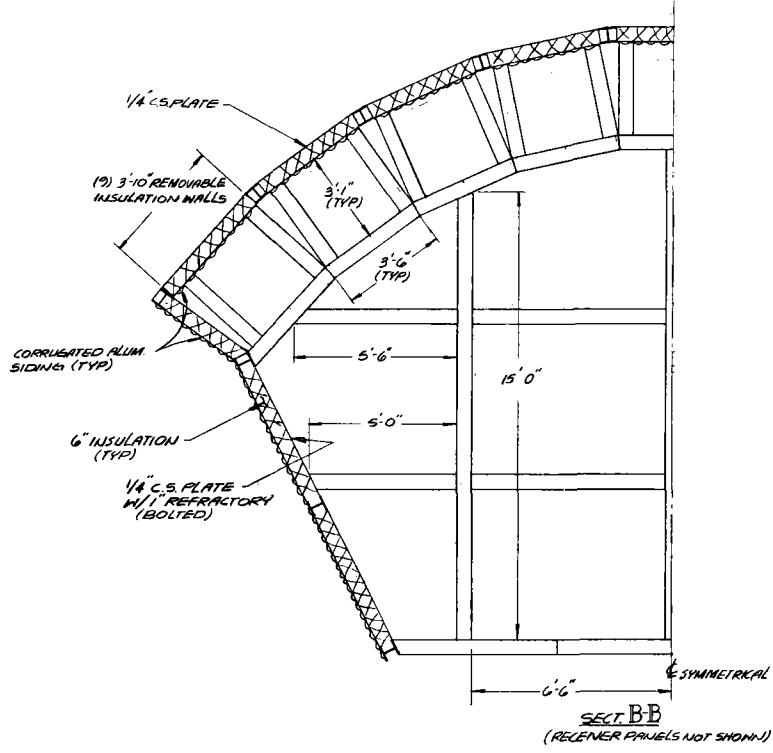
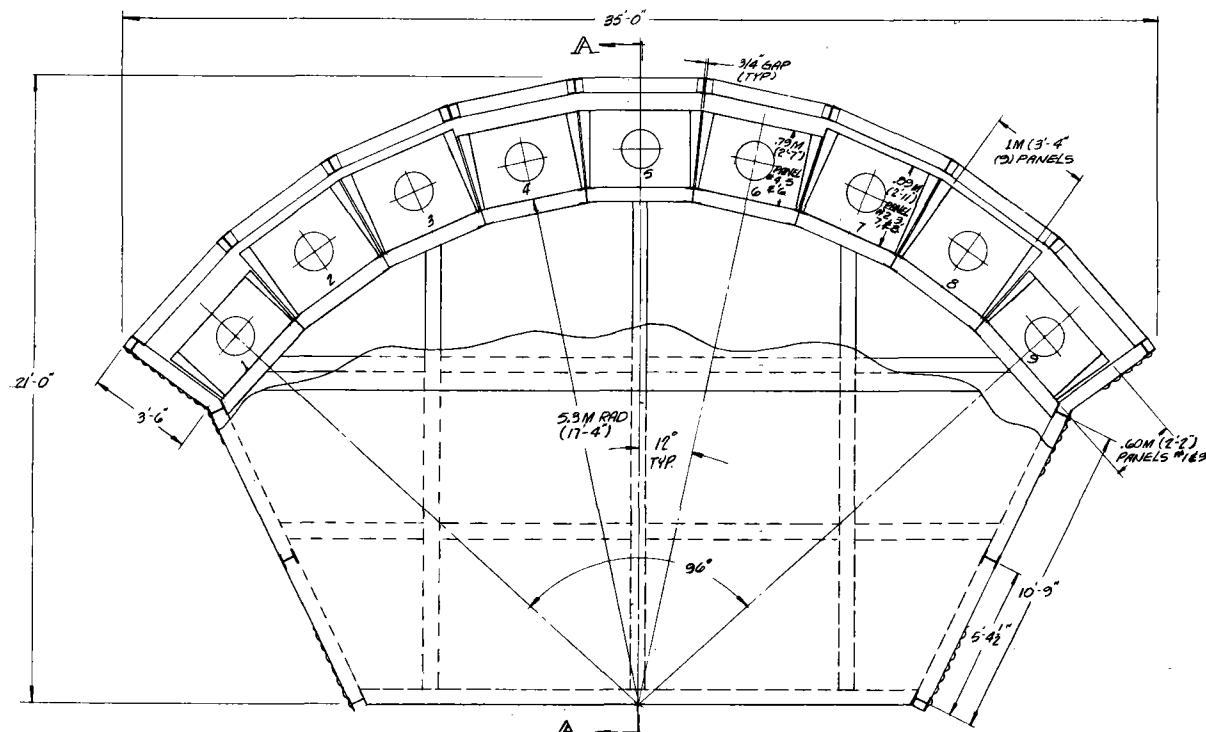
Section 10

REFERENCES

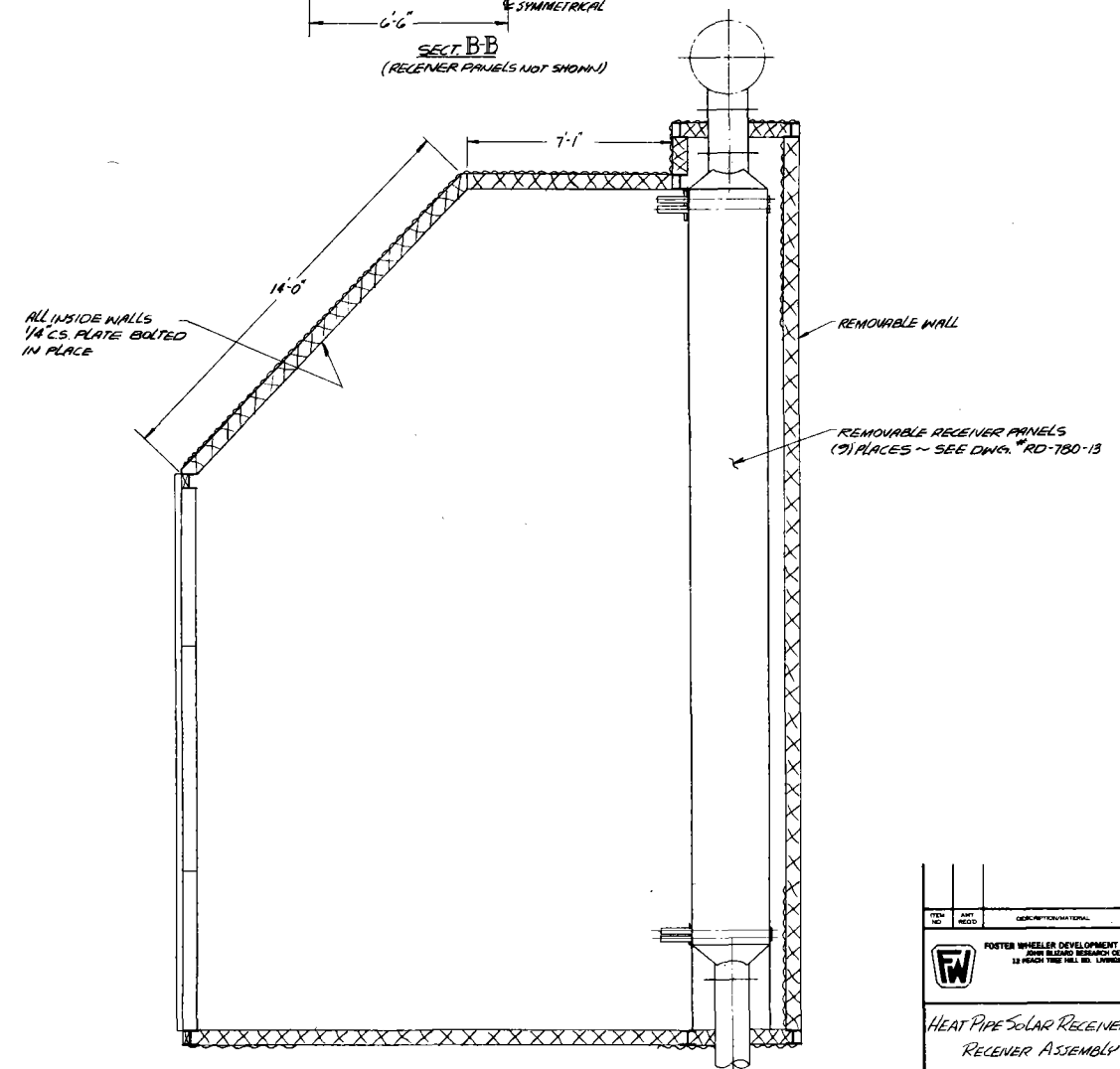
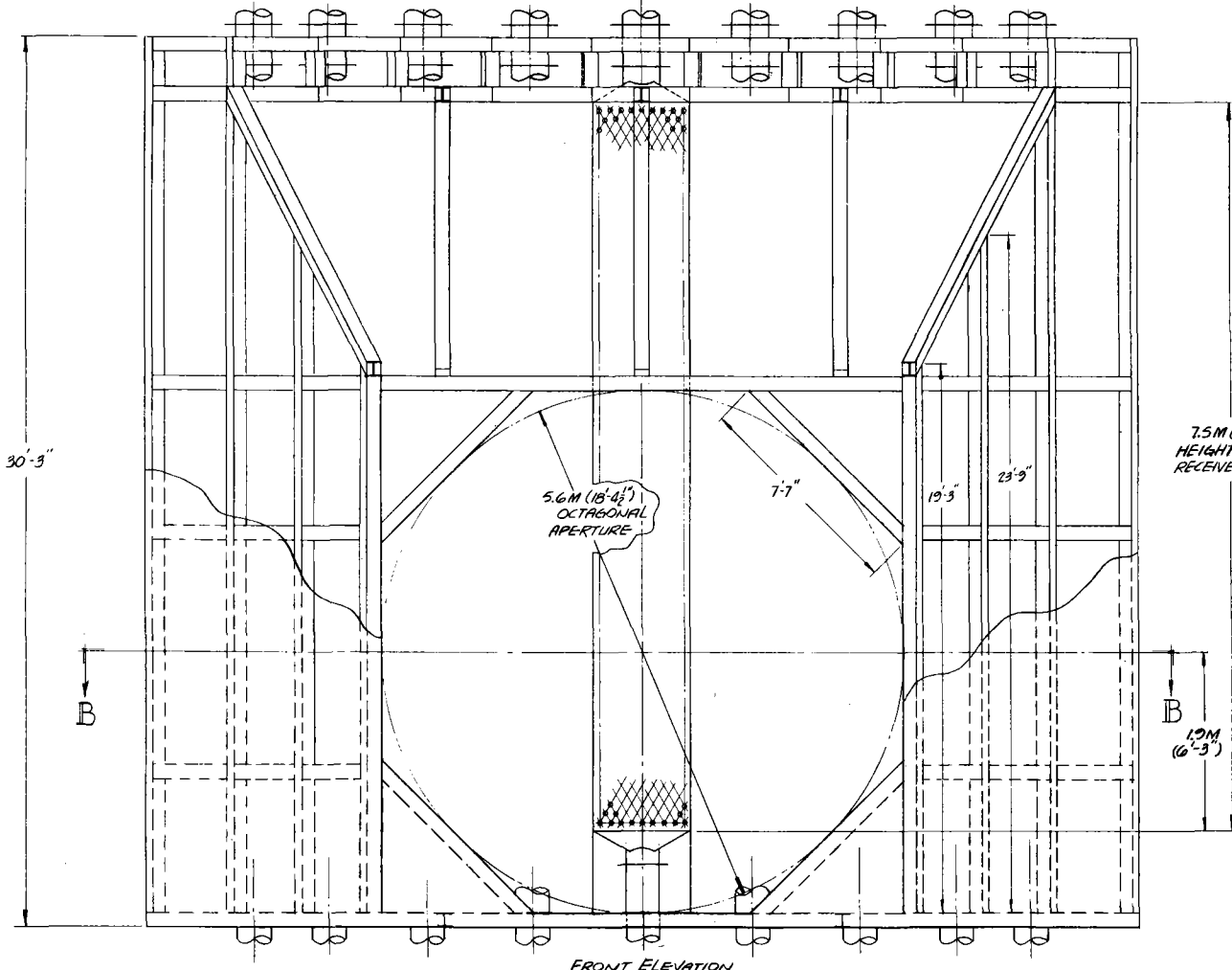
1. A. P. Fraas, "Preliminary Assessment of a Potassium-Steam-Gas Vapor Cycle for Better Fuel Economy and Reduced Thermal Pollution," Oak Ridge National Laboratory, Report No. ORNL-NSF-EP-6, 1971.
2. Martin Marietta Corporation, "Central Receiver Solar Thermal Power System, Phase 1, Quarterly Report No. 1," Report No. MCR-76-121, 1976.
3. D. H. Brown, J. C. Corman, and R. B. Fleming, "Energy Conversion Alternatives Study--Phase I Final Report," NASA Report No. CR-134948, 1976.
4. Aerospace Corporation, "Highlights of the Central Receiver Pilot Plant and Test Facility Projects," Semiannual Review," Report No. ATR-76 (7523-11)-1, 1975.
5. Martin Marietta Corporation, "Central Receiver Solar Thermal Power System, Phase 1: Preliminary Design Report, Volume 3: Collector Subsystem," Report No. SAN/1110-77-2, 1977.
6. McDonnell Douglas Corporation, "Central Receiver Solar Thermal Power System, Phase 1, First Quarterly Technical Progress Report," Report No. MDC G6318, 1976.
7. Honeywell Incorporated, "Solar Pilot Plant, Phase 1, Quarterly Report No. 1," Report No. SAN/1109-76/T1, 1976.
8. W. B. Bienert and D. A. Wolf, "Semiannual Progress Report for Heat Pipe Central Solar Receiver," Dynatherm Corporation, Report No. DTM-76-7, 1976.
9. McDonnell Douglas Astronautics Company, "Central Receiver Solar Thermal Power System, Phase 1, CDRL Item 2, Volume III: Collector Subsystem," Report No. SAN/1108-8/4, 1977.
10. D. Wolf, Dynatherm Corporation, telephone communication.
11. ASME Boiler And Pressure Vessel Code, Section VIII-Division 2, Alternate Rules, ASME, New York, 1977.
12. ASME Boiler and Pressure Vessel Code, Case Interpretations, Code Case 1592-10, ASME, New York, 1977.
13. T. V. Narayanan, G. D. Gupta, and M. S. M. Rao, "Structural Design of a Superheater for a Central Solar Receiver," to be published in Transactions of the ASME, Journal of Pressure Vessel and Piping, 1978.

14. M. S. M. Rao, "A Computer Program for Thermoelastic-Plastic-Creep Analysis of Thick-Walled Cylinders Under Nonaxisymmetric Loading," Foster Wheeler Development Corporation, Report No. EST-76-1, September 1976.
15. S. Timoshenko and J. N. Goodier, "Theory of Elasticity," 2nd ed., McGraw-Hill, New York, 1951.
16. Steel Construction, 5th ed., American Institute of Steel Construction, New York, 1962.
17. McDonnell Douglas, "Central Receiver Solar Thermal Power System, Phase 1, CDRL Item 2: Pilot Plant Preliminary Design Report, Volume VII, Book 1: Pilot Plant Cost and Commercial Plant Cost and Performance," Report No. MDC G6776, May 1977.

Appendix A

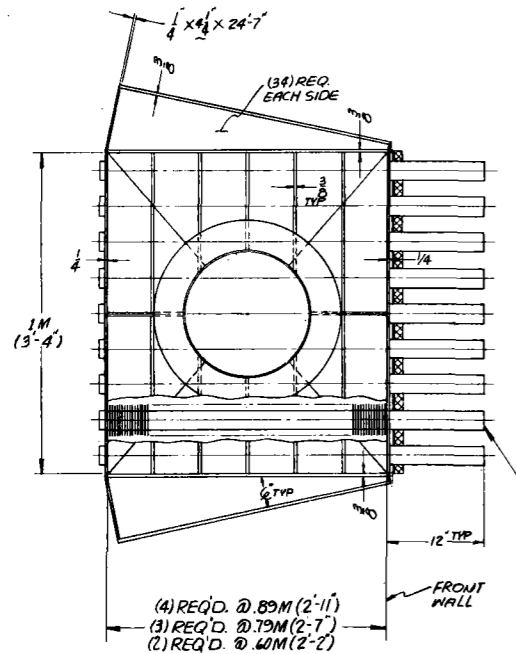
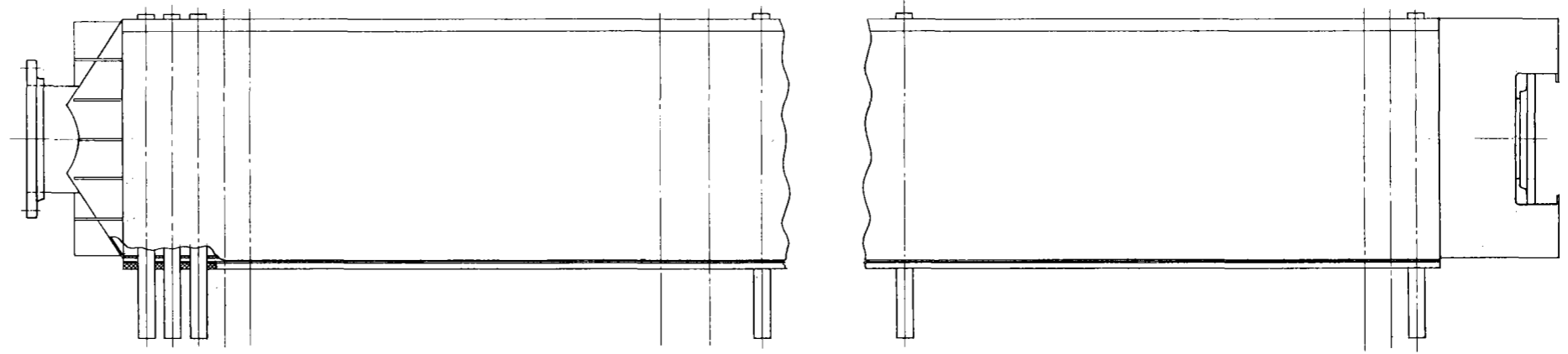
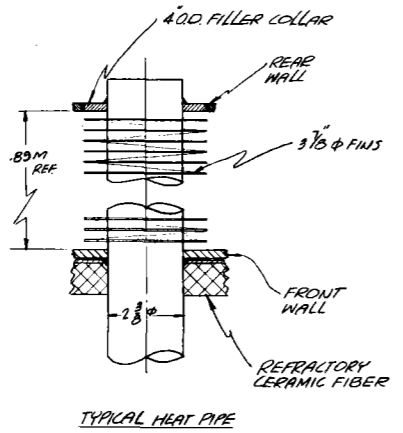


NOTES:
 1- ALL DIMS. ARE APPROXIMATE FOR ESTIMATING PURPOSE ONLY
 2- ALL FRAMING MEMBERS TO BE BEAMS, SIZE 146 X 13.5" ASTM A36 WELDED CONST.



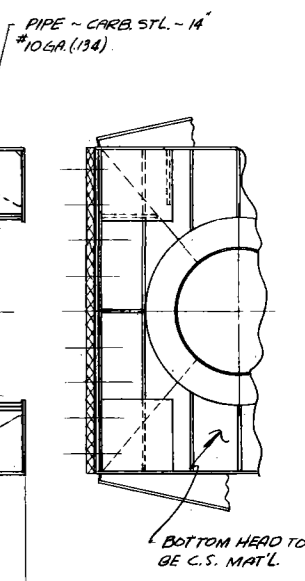
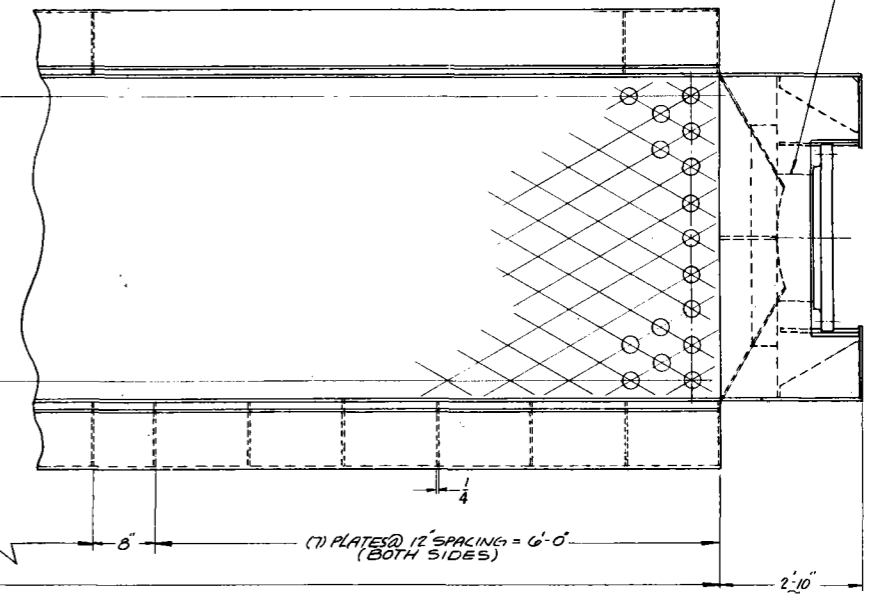
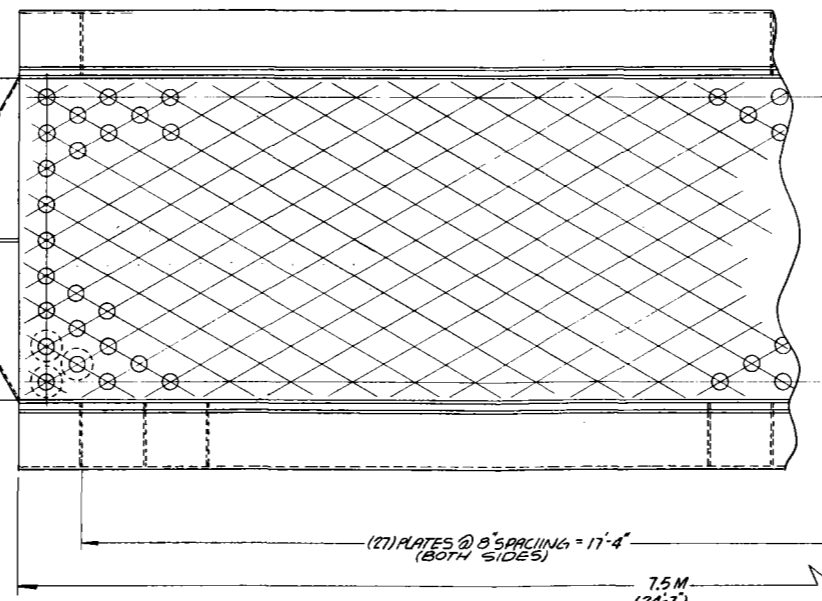
REV	DATE	DESCRIPTION	BY
FOSTER WHEELER DEVELOPMENT CORPORATION 1200 BROADWAY 12 FLOOR NEW YORK, N.Y. 10006			
HEAT PIPE SOLAR RECEIVER PLANT RECEIVER ASSEMBLY			
9-41-3411C			
DRAWN BY	ER	DATE	SCALE - 1/2" = 1'-0"
CHECKED BY	EC	DATE	
APPROVED BY	EC	DATE	RD-780-11 - L & L

NOTES:
 1- ALL DIMS ARE APPROXIMATE FOR ESTIMATING PURPOSE ONLY
 2- ALL MATERIAL TO BE INCONEL 601 EXCEPT AS NOTED

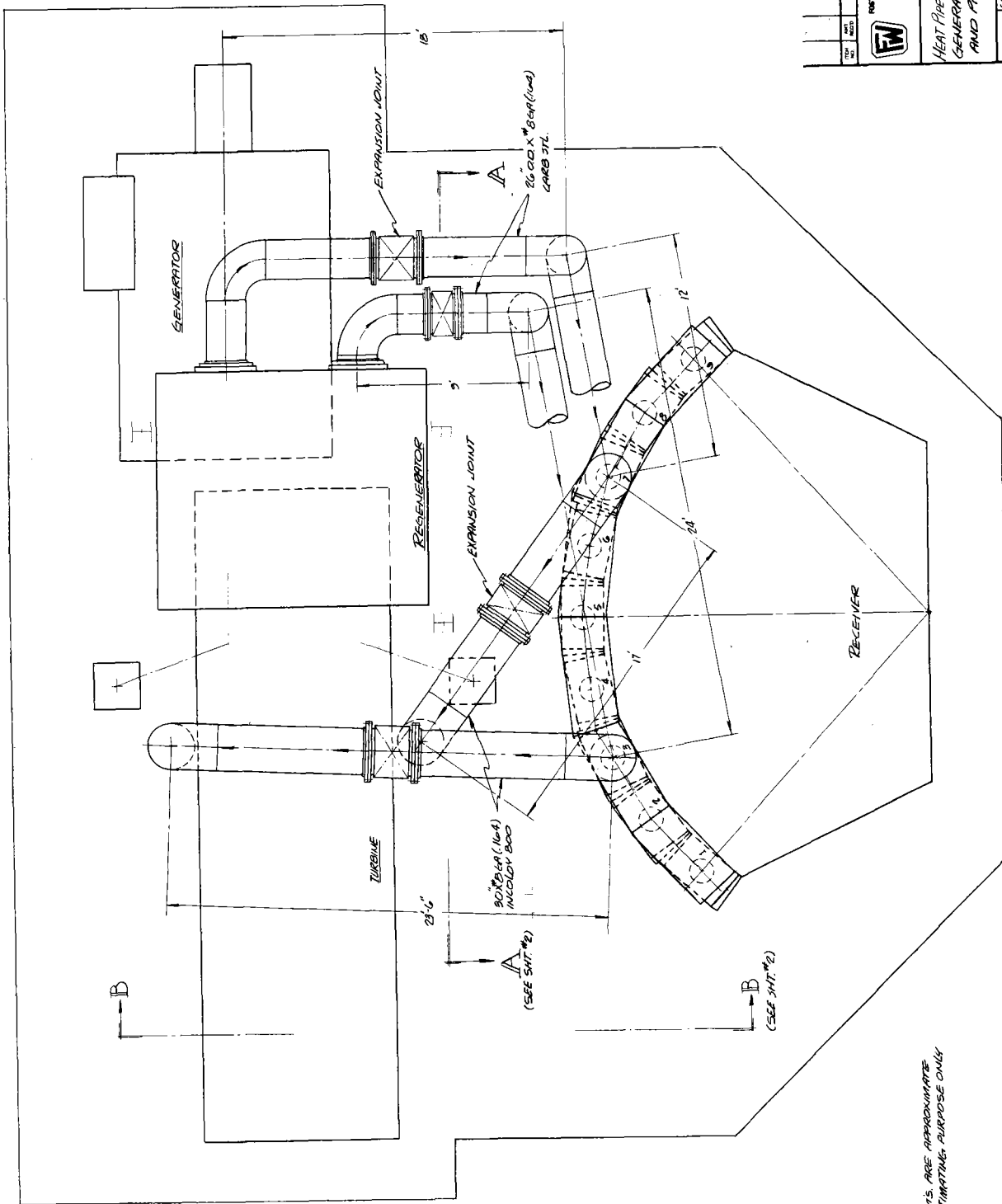


PIPE - INCOLOY 800
 16" 10GA (134)

DYNATHERM
 HEAT PIPE - 2 7/8 O.D. X 2 7/8 I.D.
 WITH 3 7/8 O.F. FINES SPACED
 (4) PER INCH
 (637) ON 4 1/2 Δ PITCH



ITEM NO.	QTY.	DESCRIPTION/MATERIAL	SIZE
FOSTER WHEELER DEVELOPMENT CORPORATION JOHN B. WHEELER RESEARCH CENTER 12 POUCH THE HILL RD. LITTLETON, CO.			
HEAT PIPE SOLAR RECEIVER PLANT RECEIVER PANELS ASSEMBLY			
2-61-94106 DRAWN BY: ER/WH CHECKED BY: EC/WH APPROVED BY: EC/WH RD-780-12			



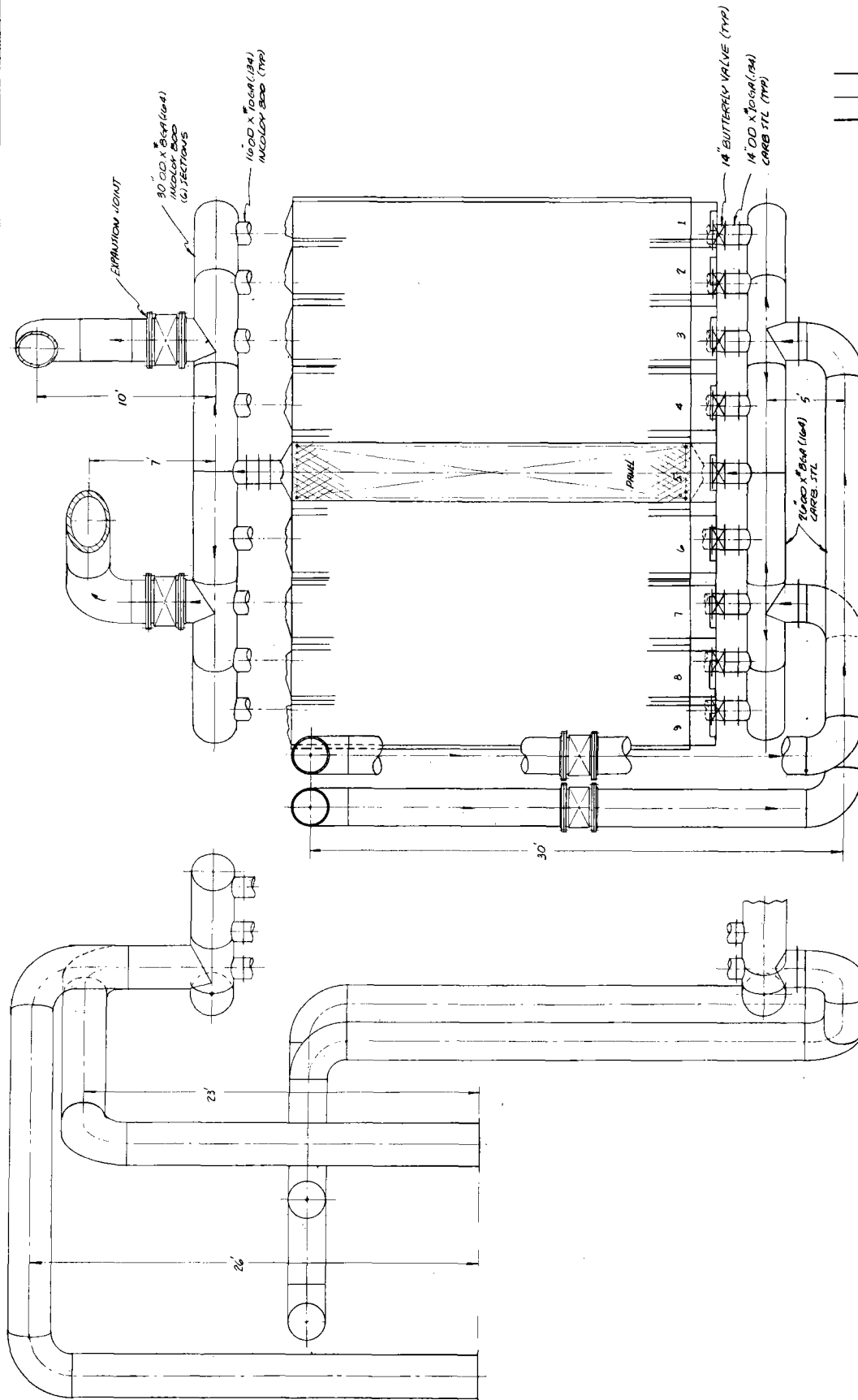
DATE	BY	APP'D	REV
9-21-54	WJ		1
10-1-54	WJ		2
10-1-54	WJ		3
10-1-54	WJ		4


PORTER WHEELER DEVELOPMENT CORPORATION
 1100 W. 10th St., Tulsa, Okla.

**HEAT PIPE SOLAR RECEIVER PLANT
 GENERAL ARRANGEMENT
 AND PIPING**

DRAWING NO. **RD-780-13** SHEET NO. **4** OF **4**


NOTES:
 1- ALL DIM'S ARE APPROXIMATE
 FOR ESTIMATING PURPOSE ONLY



DATE	REV.	BY	CHKD.
 PORTER WHEELER DEVELOPMENT CORPORATION 11 FORT STREET NEW YORK, N.Y.			
HEAT EXCHANGER RECEIVING PLANT GENERAL ARRANGEMENT AND PIPING			
SCALE	1/2" = 1'-0"	DATE	12-1-57
DRAWN BY	J. C. BROWN	PROJECT NO.	RD-180-13
CHECKED BY	J. C. BROWN	REV.	1

VIEW A-A

VIEW B-B
 (TURBINE, REGENERATOR & PANELS OMITTED)

DATE	NO.	BY	CHKD.	APP'D.	REV.
 FOSTER WHEELER DEVELOPMENT COMPANY 14 HANCOCK TRAIL RD. LUMBERTON, N.J.					
HEAT PIPE SOLAR RECEIVER PLANT PLATFORM					
SCALE	PROJECT NO.		SHEET NO.		
AS SHOWN	RD-180-14-L-1 of 4		18 of 18		



Appendix B

REPORT
ON

DYNATHERM CORPORATION

HEAT PIPE SAMPLE

ML 3495

ME 10-77-74

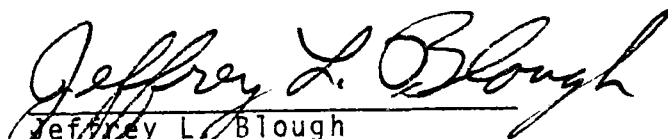
CONDUCTED AT

FOSTER WHEELER DEVELOPMENT CORPORATION
LIVINGSTON, NEW JERSEY


FILE NO: 9-41-341106-R-5002

October 7, 1977

Approved by


Jeffrey L. Blough
Manager,
Materials Technology Dept.

Prepared by


John Cocubinsky
Department Head
Metallurgical Services

FILE NO: 9-41-341106-R-5002
FROM: John Cocubinsky
TO: G. Carnasciali
CC: W. R. Applett, Jr., J. L. Blough, G. Gupta,
R. Zoschak, W. Wolowodiuk
SUBJECT: DYNATHERM CORPORATION
HEAT PIPE SAMPLE
ML 3495

INTRODUCTION

An approximately fifteen inch (15") length of a 2-1/4" O.D. heat pipe which had a measured wall thickness ranging between 0.085" and 0.110" and a 2-1/2" long section which had not been in service were submitted for investigation. Two regions (#1 and #2) on the outside surface of the longer section were encircled. Area #1 exhibited a small, predominately circumferential crack, Area #2 a roughened surface. It was reported that the roughness was developed by arcing which occurred between the pipe and the induction coil and had been induced long after the crack had formed.

The submitted pipe sample was made of Inconel 601 material. A wick and a screen which covered the entire inside surface were made of Type 304 stainless steel. Two small holes were cut into the screen, one near each end of the sample. One hole (approximately 1/4" from the crack) had been centered in the 4" induction coil. The other hole was located in that portion of the tube which was within the heat pipe condenser.

SUMMARY

The arcing at the outside surface of the tube (Region #2) resulted in a temperature sufficient high to melt the skin surface of

the tube in localized area. No cracking was detected in this region. The crack in region #1 was initiated at the inside surface of the pipe in the center of a hot spot. A small elliptical shaped region around the crack exhibited no fused metal on the surface. Two smaller intergranular cracks at the inside surface were detected at the periphery of the hot spot. A second hot spot overlapped the hot spot which contained the failure. A third hot spot on the inside surface near the heat pipe condenser section of the tube exhibited superficially deep cracks at the periphery of the hot spot. It is suggested that the failure in the tube resulted primarily from thermal stresses arising from two overlapping hot spots which were developed in the tube.

MACROSCOPIC EXAMINATION

The appearances of encircled areas #1 (crack) and #2 (arc) on the outside surface of the submitted tube may be seen in Figure 1. The appearances of the inside surface in the same portions of the tubes are depicted in Figure 2A with the screen in place and in Figure 2B after the screen had been removed. The crack appears in a light-colored metallic-appearing, elliptical-shaped area. Two roughened-surface circular areas, one overlapping the other are apparent. The appearance of the inside surface of the heat pipe condenser region with the hole in the screen may be seen in Figure 3. A stained region can be noted approximately 1" from the hole and a fused (hot-spot) area is apparent approximately 4" from the hole in the screen.

MICROSCOPIC EXAMINATION

Cross sections thru the hot-spots along the planes indicated by letters in Figures 2B and 3, a cross section at a significant distance from the hot spots, a cross section thru the rust-like indication and a cross section from the unused portion of the tube were examined microscopically. The appearance of the outside surface of the tube within the arc'ed region (location #2) is illustrated in Figure 4. The dendritic cast-metal structure on the surface shows that the metal on the surface had been molten. A surface layer approximately 0.003" deep had apparently melted as a result of the arcing.

A composite of two (2) photomicrographs illustrating the crack that penetrated the wall is exhibited in Figure 5. No evidence of fused metal can be noted at the inside surface, the origin of the crack. Two relatively shallow (approximately 0.015" deep) intergranular cracks and fused metal on the inside surface at the periphery of the hot spot in which the failure developed are depicted in Figure 6 (top). Shallow cracks and fused metal on the inside surface within the hot-spot which was near the condenser end of the tube may be seen in Figure 6 (bottom). Recrystallization of the grains at the surface is apparent. The microstructure in a region at a significant distance from the hot spots is illustrated in Figure 7 top and a similar appearing structure presented in Figure 7 bottom is representative of the microstructure of the unused portion of the tube.

DISCUSSION

Examination of the submitted sections of the heat pipe revealed that in addition to the failure, secondary cracking had developed at the periphery of hot spots. The failure was in the form of a single crack which apparently had followed an intergranular path of propagation, the same mode as the secondary cracks. The surface of the small elliptical-shaped area about the failure which was in the center of a hot spot on the inside surface had not been molten although the surrounding area of the hot spot had exhibited fused metal.

It would appear that the development of hot spots and fusion of metal on the inside surface of the heat pipe generated thermal stresses of sufficient magnitude to induce intergranular cracks. The hot spots on the inside surface developed metal temperatures of approximately 2600°F. Upon cooling, a crack was initiated in the center of one hot spot and then an overlapping hot spot introduced a stress which propagated the crack, possibly to failure.

No signs of metal deterioration in the form of cracking or creep voids was detected in any region outside the hot spots. It is apparent that the heat pipe would have been satisfactory for continued service, if hot spots had not developed cracks on the inside surface of the pipe.

CONCLUSIONS

It is the opinion of this laboratory based upon an evaluation of the submitted section of the heat pipe that:

1. The skin of the pipe in hot spots developed on the inside surface reached temperatures of 2600°F.

2. A crack was initiated at the center of one hot spot. The surface at this crack was not fused indicating that the center of the hot spot was colder than the surrounding area.

3. A second hot spot, overlapping the first, propagated the crack.

4. Intergranular cracks were developed at the periphery of all hot spots.

5. All regions not subjected to arcing were sound.

6. The pipe would have performed satisfactorily if no hot spots had been formed.

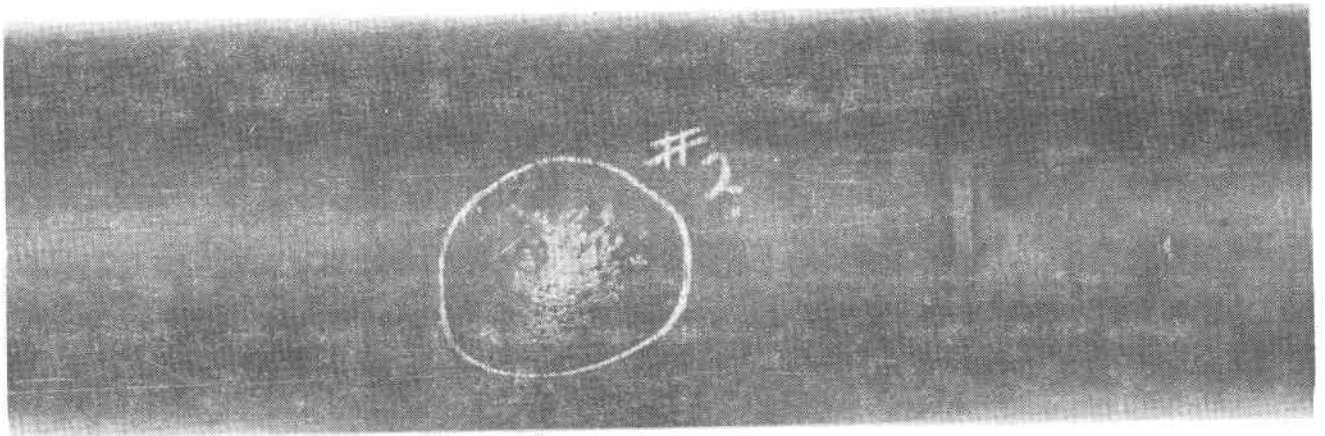
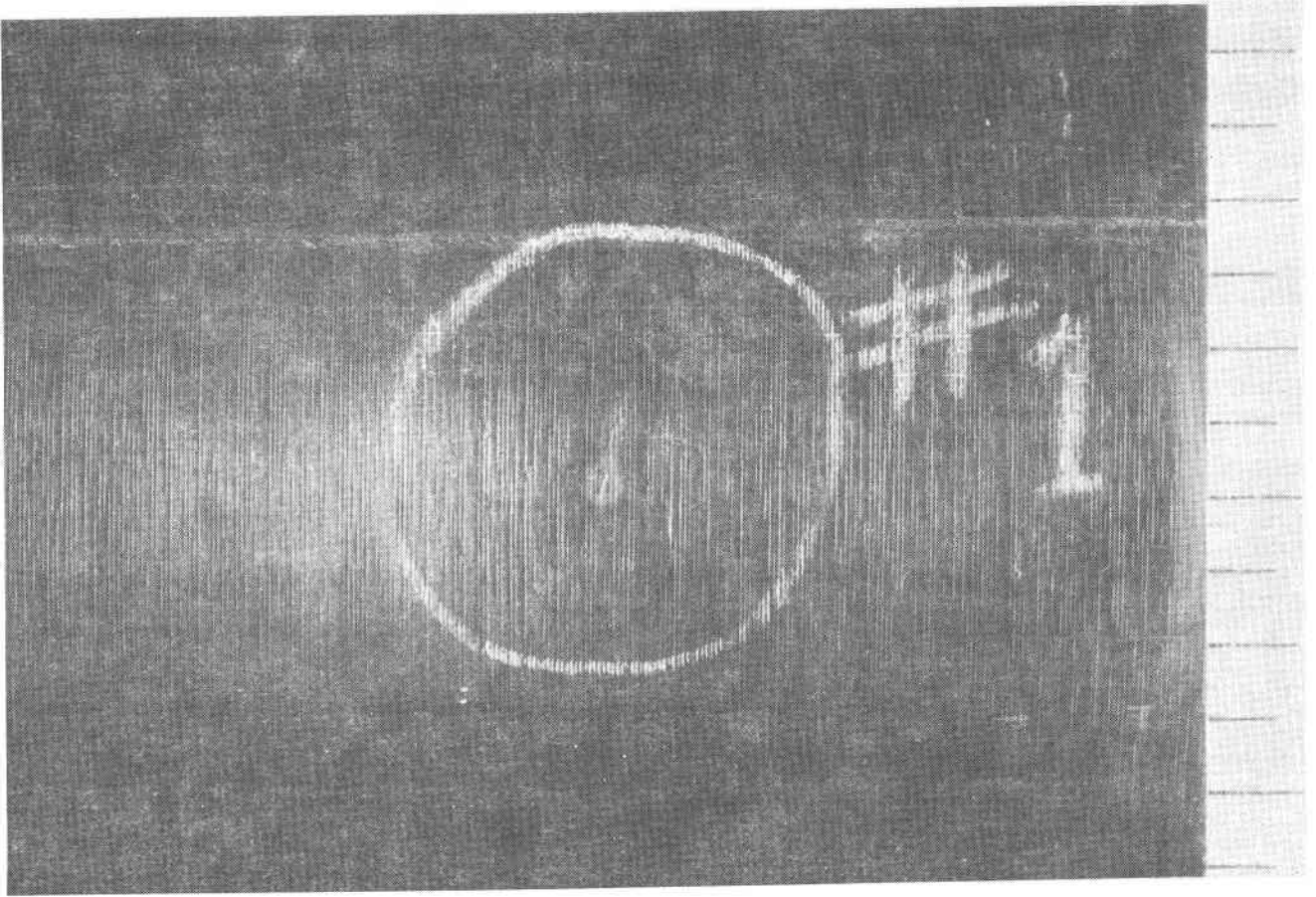


FIGURE 1

TOP:	PHOTOMACROGRAPH	3X MAGNIFICATION	AS RECEIVED
BOTTOM:	PHOTOMACROGRAPH	1X MAGNIFICATION	AS RECEIVED

The appearances of two encircled regions on the outside surface of the submitted tube section are shown. A faint crack can be noted in the center of Circle #1.

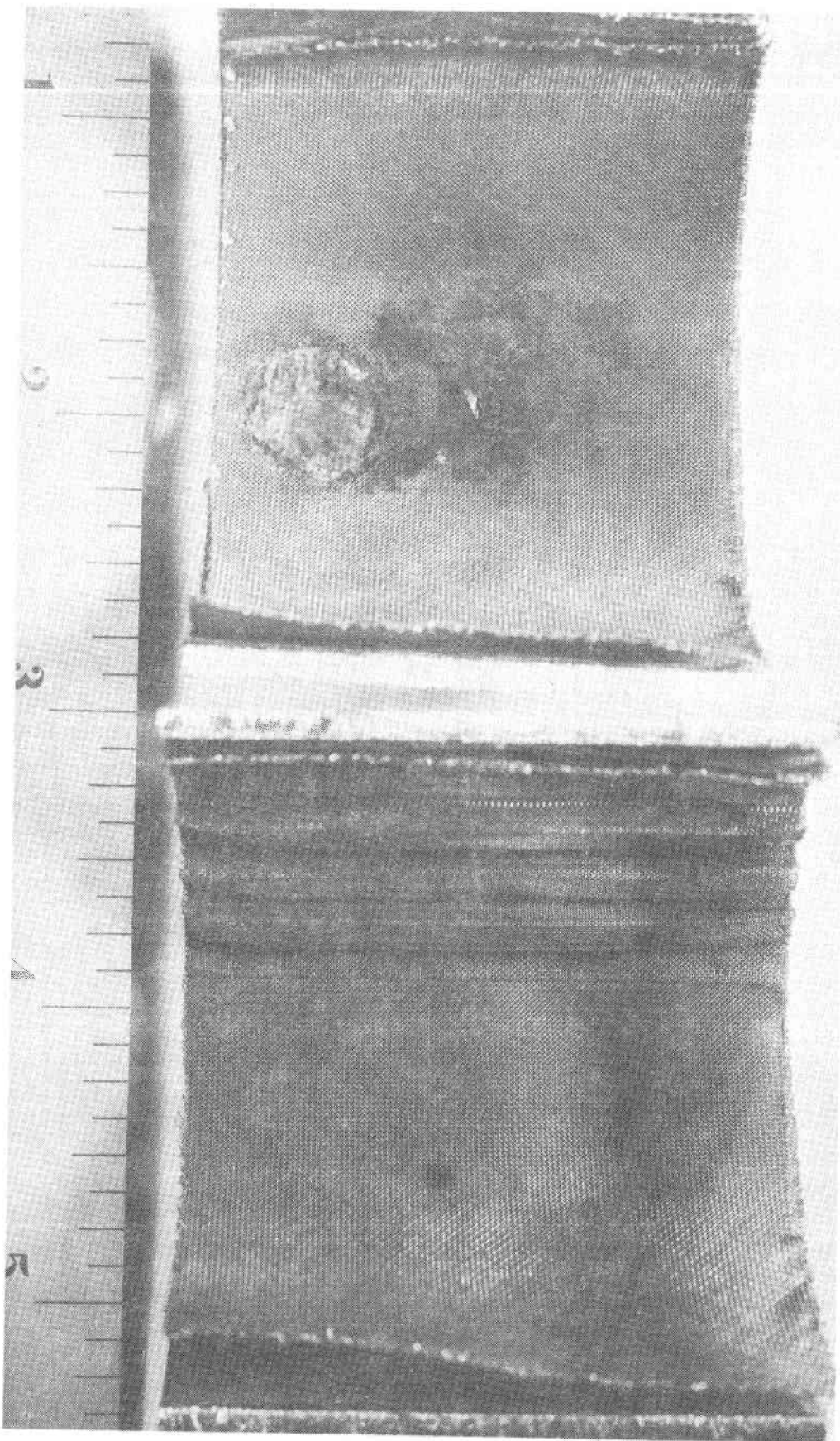


FIGURE 2A

PHOTOMACROGRAPH

2X MAGNIFICATION

The appearance of the inside surface below encircled areas #1 (top) and #2 bottom are shown.

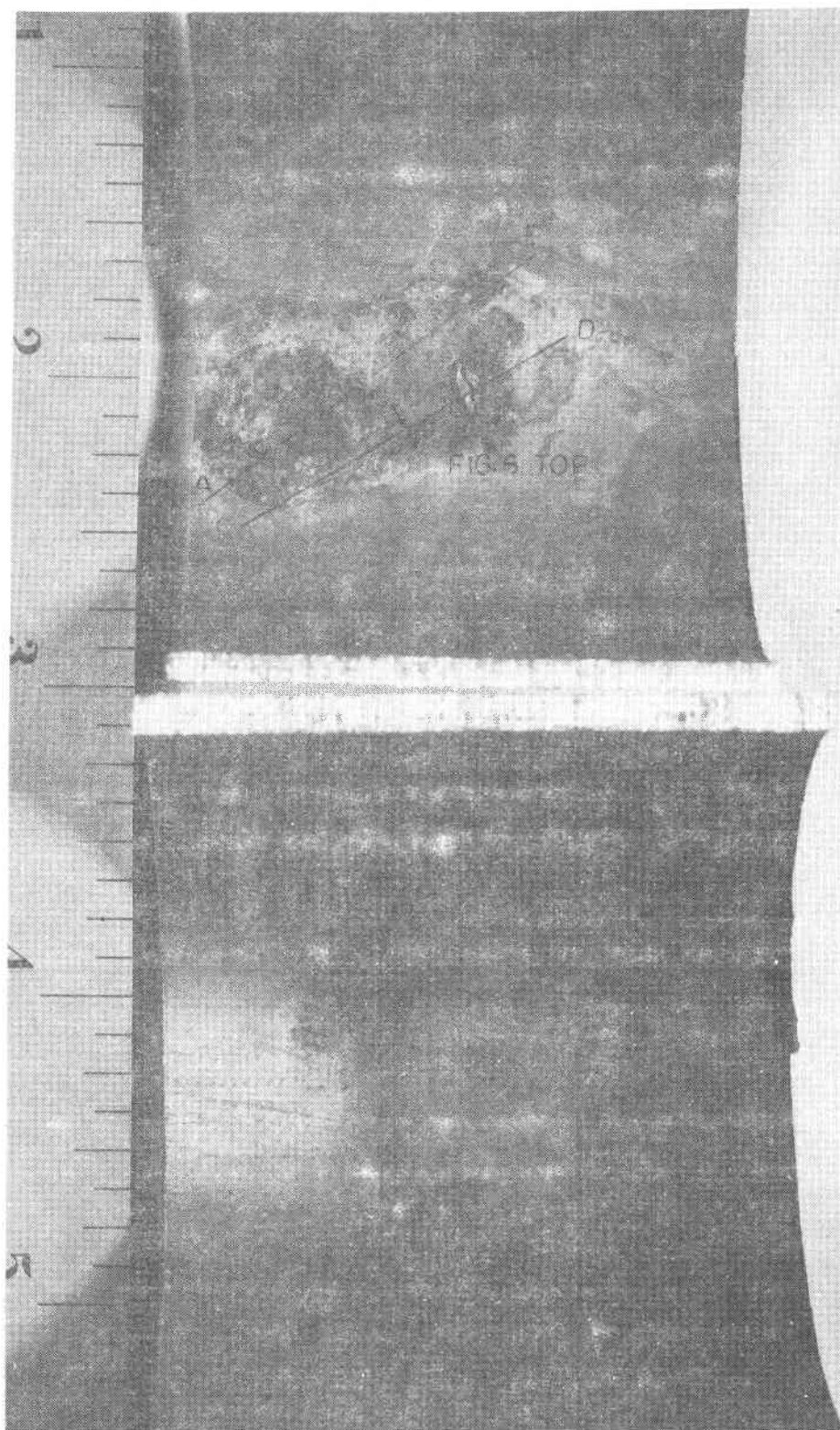


FIGURE 2B

PHOTOMACROGRAPH

2X MAGNIFICATION

Same as Figure 2A after screen had been removed. The crack is clearly visible. It appears that the crack is near the center of one of two hot spots. The elliptical light-colored surface around the crack was smooth and metallic-appearing. Cross sections thru the planes indicated by A-B and C-D were removed for microscopic examination. Two small intergranular cracks (shown in Figure 6) were at the site located by the arrow.

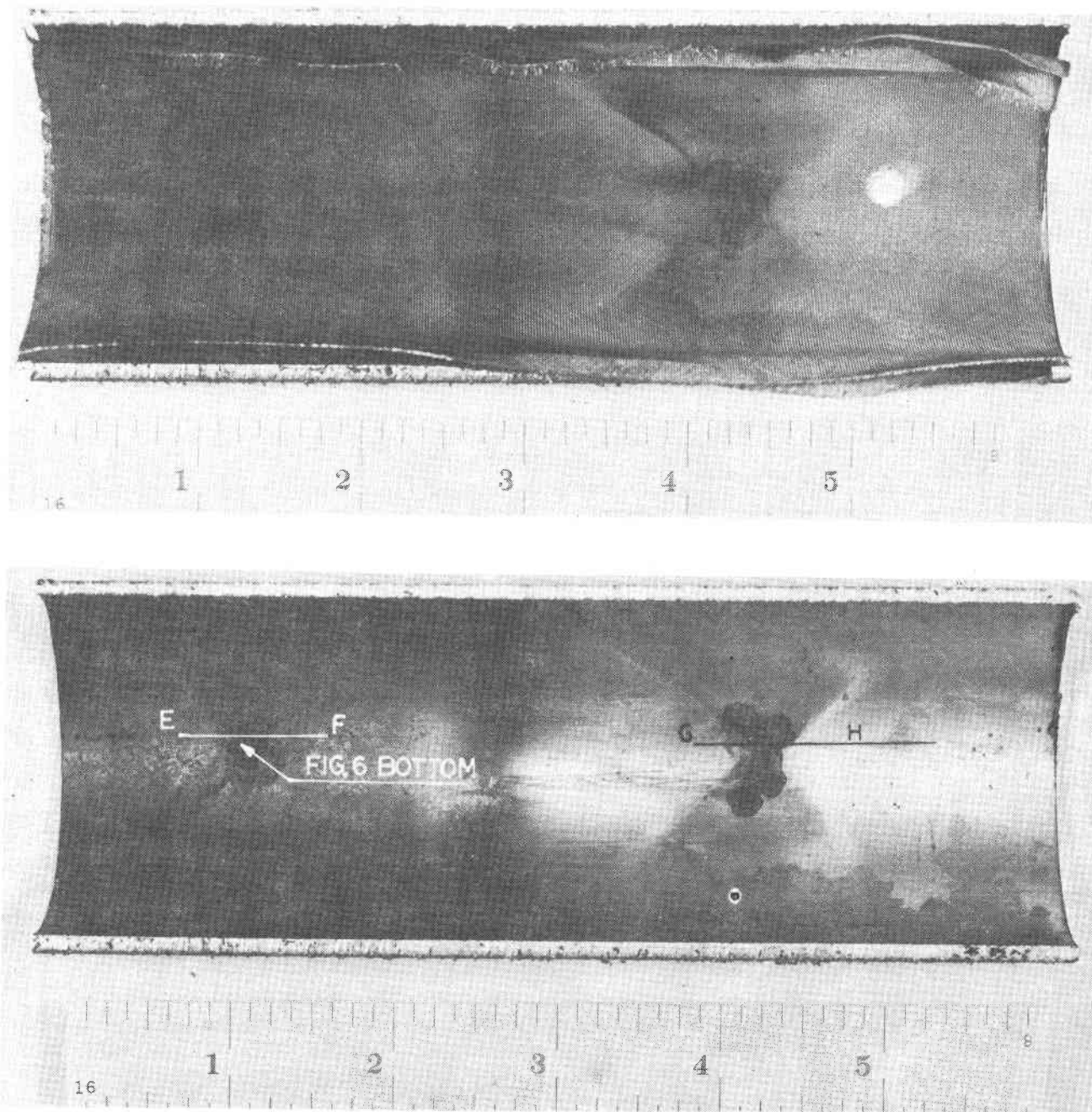


FIGURE 3

PHOTOMACROGRAPH

1X MAGNIFICATION

The inside surface (with the screen in place-top) at the opposite end of the tube exhibited hot spot (at left) and a reddish rust-like stain near the hole. Cross sections thru the planes indicated by E-F and G-H were removed for microscopic examination. Minor intergranular cracking (shown in Figure 6 bottom) was noted at the site located by the arrow.

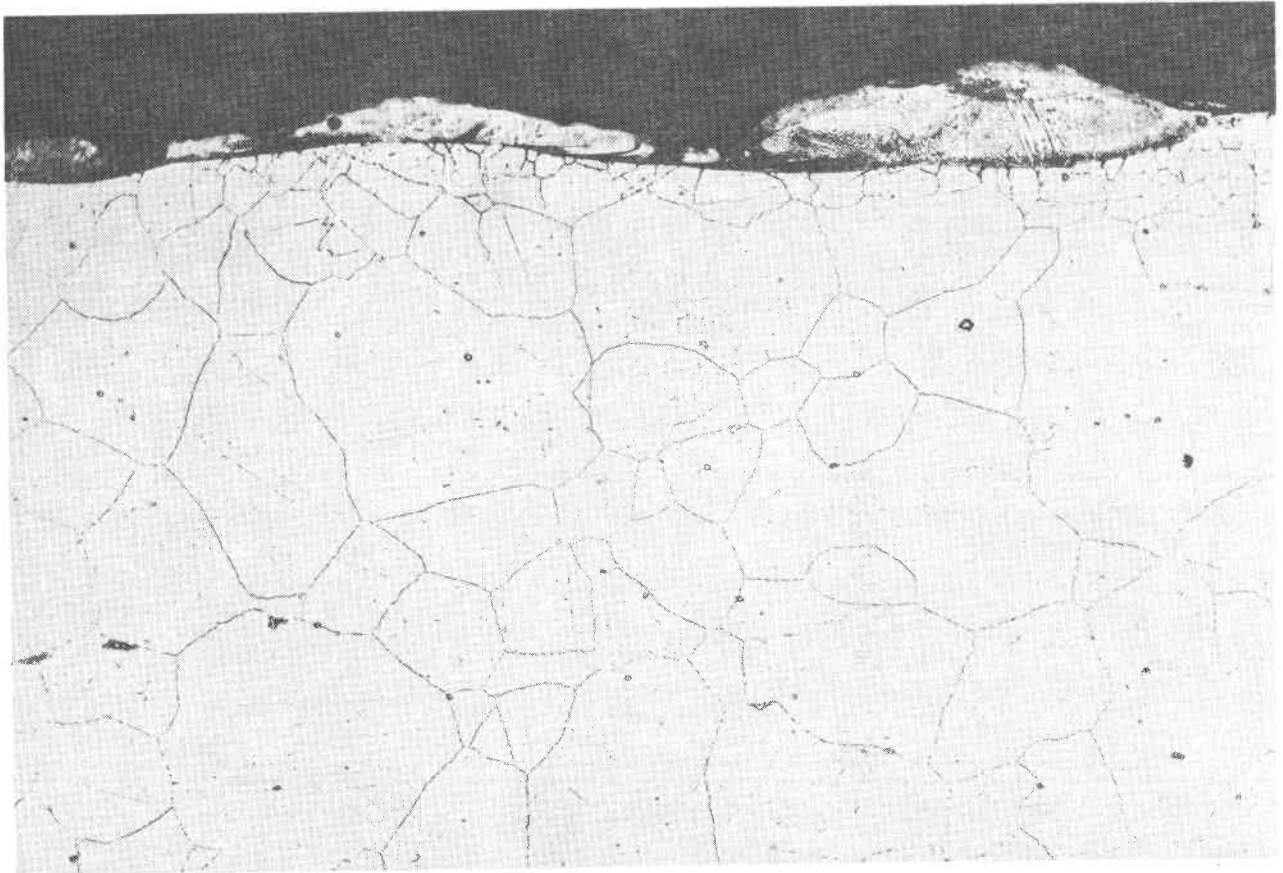


FIGURE 4

PHOTOMICROGRAPH 100X MAGNIFICATION ELECT. OXALIC ACID ETCH

The appearance of the outside surface within encircled area #2 is shown. The greyish, mottled islands on the surface is fused metal.

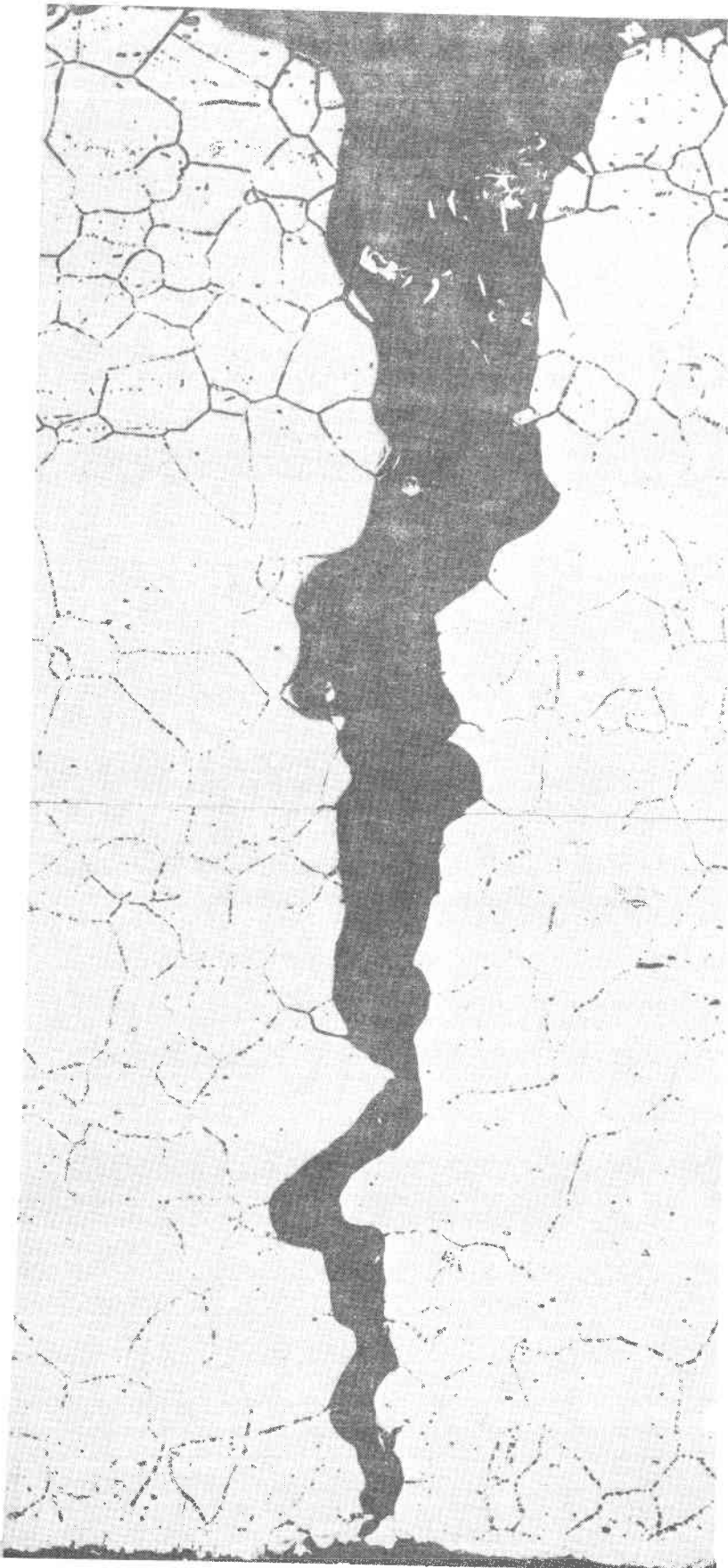


FIGURE 5

PHOTOMICROGRAPHS 100X MAGNIFICATION ELECT. OXALIC ACID ETCH

A composite of two photomicrographs showing the crack thru the tube wall at location #1 is shown. The inside surface (upper edge) was not covered with fused metal.

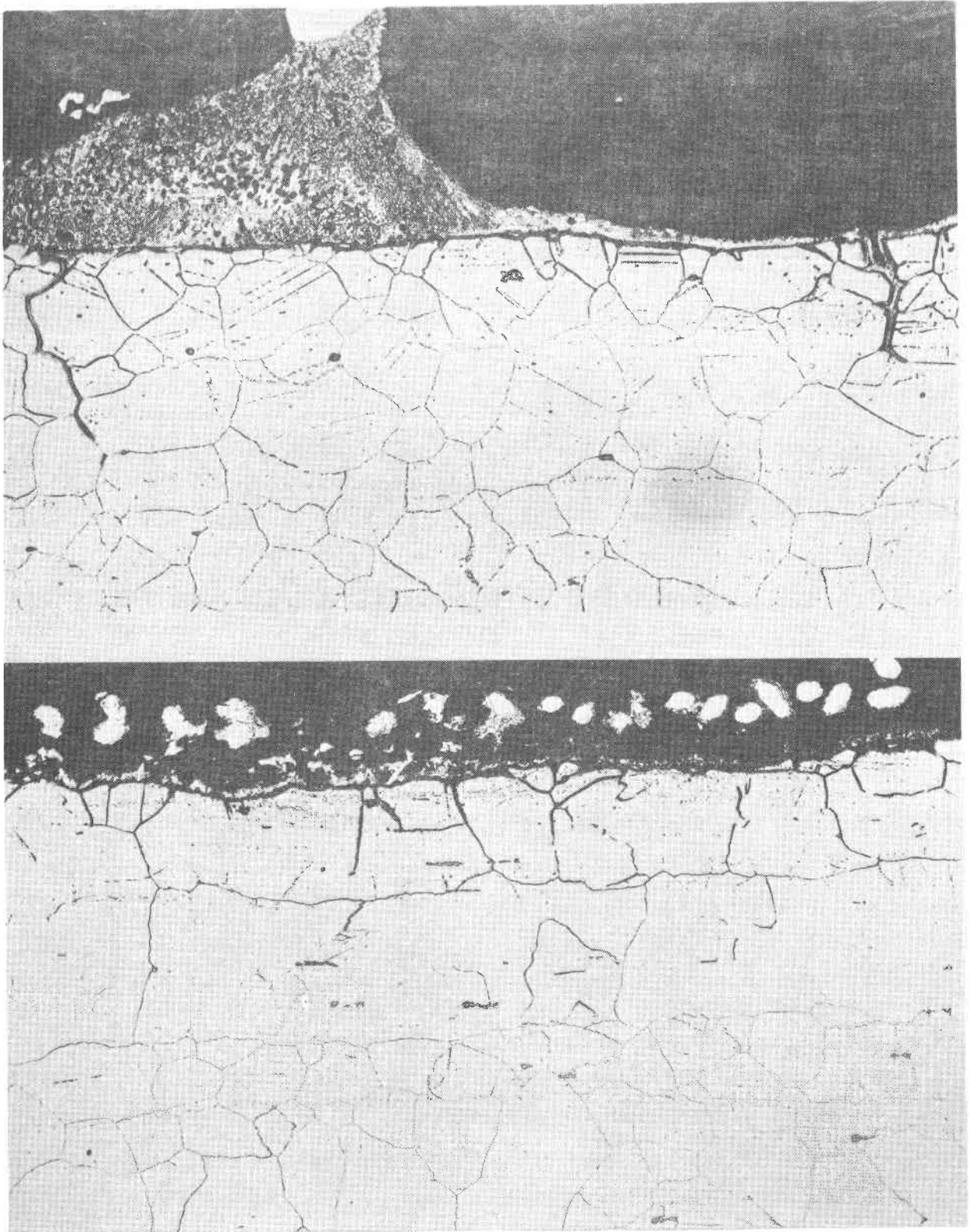


FIGURE 6

PHOTOMICROGRAPHS

100X MAGNIFICATION

ELECT.OXALIC ACID ETCH

TOP: Fused metal on the inside surface at the periphery of a hot-spot region (location #1) and two shallow intergranular cracks (near the left and right edges) are shown.

BOTTOM: Fused metal on the inside surface and minor intergranular penetration at a hot-spot is shown. Grain growth can be noted at the surface.

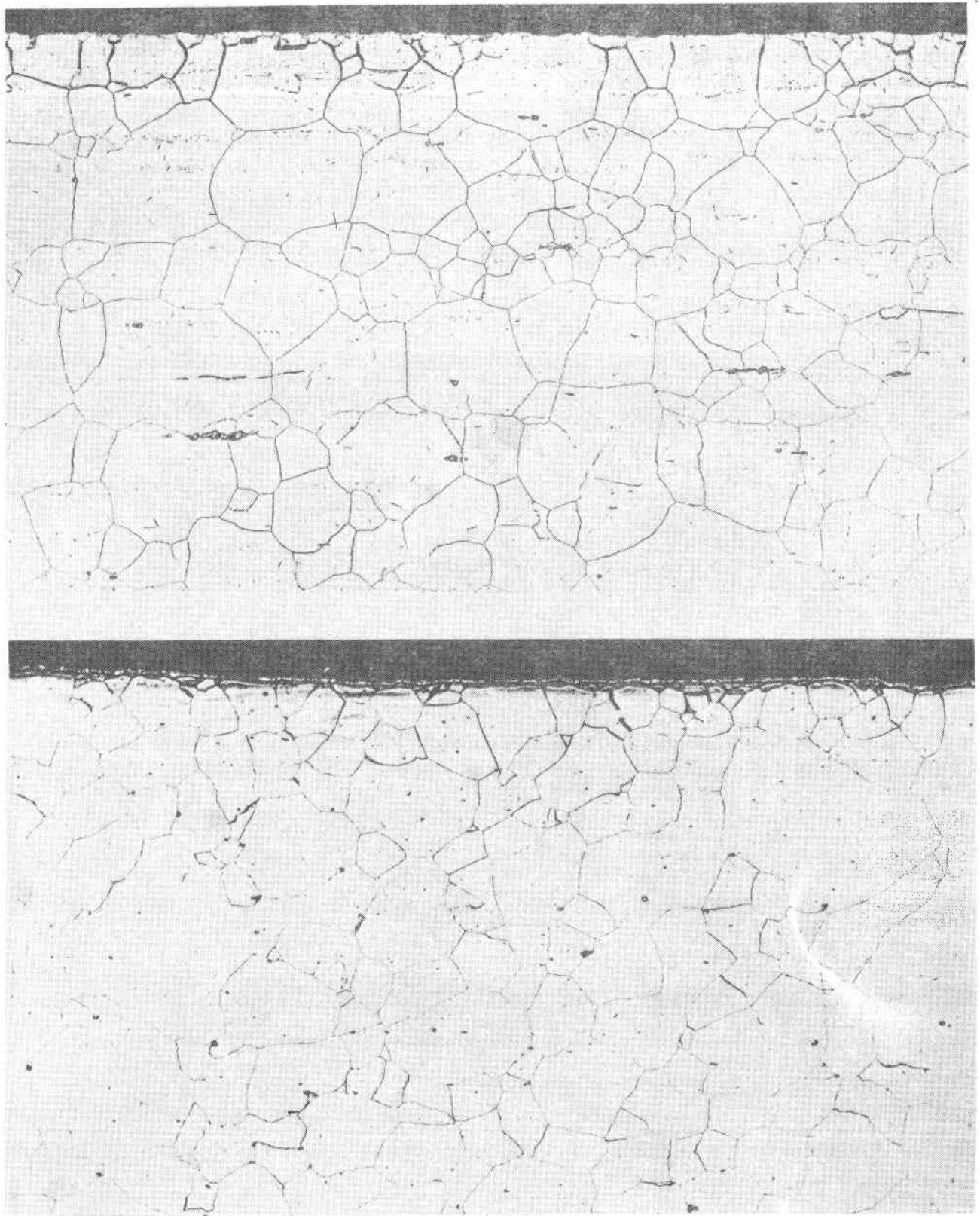


FIGURE 7

PHOTOMICROGRAPHS 100X MAGNIFICATION ELECT.OXALIC ACID ETCH

TOP: The structure of the tubing material in regions away from the hot-spots is shown.

BOTTOM: The as-received structure of the material which had not been in service is shown.

B-14

UNITED STATES DEPARTMENT OF ENERGY
P.O. BOX 62
OAK RIDGE, TENNESSEE 37830

OFFICIAL BUSINESS
PENALTY FOR PRIVATE USE \$300

POSTAGE AND FEES PAID

UNITED STATES
DEPARTMENT OF ENERGY



FS- 1

SANDIA LABORATORIES
ATTN TECHNICAL LIBRARY
LIVERMORE, CA 94550